STRUCTURAL AND FUNCTIONAL CHARACTERIZATION OF THE SURFACE LAYER OF CAULOBACTER CRESCENTUS

by

JAN MERTENS

Master, University of Leuven, Belgium, 2009

A THESIS SUBMITTED IN PARTIAL FULFILLMENT OF
THE REQUIREMENTS FOR THE DEGREE OF

MASTER OF SCIENCE

in

THE FACULTY OF GRADUATE STUDIES

(MICROBIOLOGY AND IMMUNOLOGY)

THE UNIVERSITY OF BRITISH COLUMBIA

(Vancouver)

MAY 2012

Abstract

Proteinaceous surface layers (S-layers) have been identified in hundreds of different species belonging to all major phylogenetic groups of Bacteria and most Archaea and form a geometrically arranged paracrystalline lattice. Despite their wide abundance, few structural and functional studies have been performed on S-layers. Obtaining high-resolution structural models has been hampered by the aggregation properties of S-layers, whereas only a few functions have been identified. This thesis focuses on the structure and the function of the hexagonal S-layer of the environmental bacterium *Caulobacter crescentus*. In the first part of my thesis, an array of new methods was devised and tested to stabilize the S-layer protein (RsaA). Protein concentrations of an N-terminally truncated protein ($RsaA_{\Delta 0\text{-}222}$) could be increased up to 7 mg/mL while maintaining the protein in the monomeric form. Stable protein samples were found to crystallize in the presence of Ca^{2+} and Sr^{2+}. However, crystals were not thick enough (mainly formed in two dimensions), as x-ray diffraction experiments showed diffraction patterns with low resolutions. Hence, obtaining high-quality crystals remains a challenge. The second part of my thesis demonstrates that the S-layer serves as a resistance mechanism to cationic antimicrobial peptides, which are produced by virtually all living organisms, including bacteria, fungi, plants and animals. S-layer positive strains were shown to be less susceptible to antimicrobial peptides than S-layer negative strains in MIC and killing assays. This protective effect was also observed when S-layer positive and negative strains were grown in biofilms. S-layer mediated resistance to antimicrobial peptides was further confirmed using epifluorescence microscopy. Addition of exogenous S-layer protein significantly increased the resistance of an S-layer negative strain to antimicrobial peptides. Overall, these results identify a new, previously unrecognized role for the S-layer as a resistance mechanism against antimicrobial peptides.

Preface

Some experiments in chapter 3 were part of a collaboration: the initial nanobody procedures to obtain 10 Nbs that bind RsaA were performed in the lab for Structural and Molecular Microbiology (Han Remaut, University of Brussels), x-ray diffraction experiments were performed together with Dr. Anson Chan (Murphy lab, University of British Columbia). I performed all the other experiments completely myself.

The work in chapter 4 was performed in collaboration and has been accepted for publication in 'Applied and Environmental Microbiology':

de la Fuente-Núñez C.[#], Mertens J.[#], Smit J. and Hancock R.E.W. (# these authors contributed equally to this work). Bacterial surface layer protects against antimicrobial peptides.

For each experiment, the individuals who performed the work are acknowledged below.

I and C. de la Fuente-Núñez contributed equally to the MIC assays, growth curve and killing assays. The biofilm staining was done by C. de la Fuente-Núñez. I performed the double fluorescence labelling assays. Exogenous S-layer protein was prepared by me and the MICs were determined together with C. de la Fuente-Núñez.

Table of contents

List of tables

List of figures

List of abbreviations

B-LL37	Biotinylated LL37
BSA	bovine serum albumin
CFU	colony forming unit
CV	column volume
DLS	dynamic light scattering
EM	electron microscopy
FITC	fluorescein isothiocyanate
HIV	Human Immunodeficiency Virus
HRP	horse radish peroxidase
IPTG	isopropyl β-D-1-thiogalactopyranoside
LB	Luria Bertani
MCS	multiple cloning site
Nb	nanobody
OD_{600}	optical density measured at 600 nm
PBS	Phosphate Buffered Saline
PCR	Polymerase Chain Reaction
pI	Isoelectric point
PYE	peptone yeast extract
RPM	revolutions per minute
RT	room temperature
S-layer	surface layer
SLPS	smooth lipopolysaccharide
SDS-PAGE	sodium dodecyl sulfate polyacrylamide gel electrophoresis

TBS	Tris Buffered Saline
WT	Wild Type

Acknowledgements

This thesis is the cherry on the cake of my time as Master's student in Microbiology and Immunology at UBC. However, reaching this would not have been possible without the support and guidance of other people. Therefore I would like to thank everyone for their contributions.

Foremost I'd like to express my thanks to Dr. J. Smit, for giving me the opportunity to work on the S-layer of his *Caulobacter* and who always closely followed up my thesis and supplied me with his ideas. I am grateful to the other lab members: Dr. J. Nomellini for sharing his indispensable guidance throughout the whole course of my thesis, Mike for his scientific input and enthusiasm, Lyn for her help when I started, Mihaela, Lucia, Martin, Angie, Heidi, Vivian, Sas, Evan, Christina and Amanda. My gratitude goes also towards my two committee members, Dr. M. Murphy and Dr. R. Fernandez who have always surveyed my thesis with much interest and supported it with fruitful suggestions.

I am also thankful to all the people I collaborated with: R. Hancock for his input and support for the peptide work, Dr. H. Remaut for his contribution with the Nanobodies. Special thanks go also to my collaborator César, for his invaluable friendship and support. And I also like to acknowledge Dr. Anson Chan and Angele for always sharing their expertise with a smile.

Many thanks go to all my other friends and colleagues: Alexander, Bieke, Franz, Sarah, Liz, Elena, other Jan, Darlene and everybody else that was there during these past years.

I definitely want to thank my girlfriend Susana, for being there during hard and good times, and always helping wherever she can.

Finally I would like to thank my parents for giving me the opportunities, supporting my study choices and for standing by my side during my enlightening and sometimes crazy journey in Vancouver.

1. Introduction

1.1 S-layers

1.1.1 From a simple curiosity to a challenging new research field

Surface layers (S-layers) are common cell surface structures that are present in a wide range of bacterial species and almost all Archaea. They are built up out of protein or glycoprotein subunits that form a paracrystalline lattice, which is attached to the microorganism and covers it completely.

S-layers were first discovered by Houwink and Le Poole in 1952. When they examined bacterial cell wall fragments of *Spirillum serpens* by using electron microscopy, they observed protein particles that were organized into a hexagonal pattern [3]. A couple of years later, Houwink also noticed S-layers in the archaon *Halobacterium salinarium* [4]. Initially, the importance was underestimated because S-layers had not been observed in model organisms such as *Escherichia coli* or *Bacillus subtilis*. However, beginning in the mid-eighties, S-layers were detected and characterized in a wide range of bacterial species and were found to be an essential cell wall structure for almost all *Archaea* and thereby, interest in the S-layer field was renewed.

S-layers of some bacteria, such as the Gram-negative model organism *Caulobacter crescentus*, can easily be genetically manipulated and could be further developed into a biotechnological platform for both medical and nanotechnological purposes. However, the main road block that has slowed researchers during the past decades, is related to the S-layer proteins themselves. Even though S-layers are very diverse among species, all S-layer proteins characterized are highly unstable when isolated, which hampers their use. More importantly, the instability is a major obstruction for obtaining structural data on an atomic level. A high-resolution three-dimensional structure of the S-layer is essential in order to develop it into a high-end technology platform.

The first part of this thesis concerns trials to overcome the protein-instability problems of S-layer proteins. Using *C. crescentus* as a model organism, I developed and evaluated several

new strategies to stabilize protein behavior and used this knowledge to further tackle the structure problem (see **1.2.2)**.

Another enigma rises when it comes to assigning a function to S-layers. Some specific functions were found, and more often hypothesized for certain bacterial S-layers. Moreover, if it exists, a common function for all bacterial S-layers has not yet been revealed and a huge hiatus in our knowledge still exists as a whole list of functions in their environmental context, has yet to be tested. The second part of my thesis is dedicated to research into the function of S-layers. Based on the findings in my thesis, I propose a new hypothesis for S-layer function: S-layers offer Bacteria protection to antimicrobial peptides (see **1.3.2**)

1.1.2 Examples of S-layer applications

A protein that is displayed at very high densities and is organized in a geometrically defined lattice on a bacterial surface, opens the door to biomedical and nanotechnological applications. The S-layer of Gram-positive bacteria (e.g. *Geobacillus staerothermophilus*, *Lysinibacillus sphaericus*) can be recrystallized on solid supports, which can serve as an immobilization surface for nanoparticles. Biosensors, ultrafiltration membranes and immuno-assays have been designed using this platform[1,5]. In the context of this thesis, I will focus on the applications established with the S-layer of the Gram-negative *C. crescentus*. All these applications utilize the bacterium with its S-layer surface. The protein that forms the S-layer was found to tolerate a variety of heterologous peptide inserts at certain locations. Expression of a protein G IgG-binding domain in the S-layer was used as a highly sensitive antibody bio-assay [6]. The S-layer is also potentially useful to prevent HIV infection. Displaying molecular compounds of the HIV/host cell complex (e.g. MIP1α, domain 1 of CD4) reduced infectivity, and even more by co-display [7]. The authors also showed that display of HIV-specific antibodies could be used to neutralize HIV. Co-display of the mammalian CD4-receptor or HIV antibodies that bind epitopes formed by binding of HIV to CD4, did also increase HIV neutralization [8]. Another example of the versatility of S-layer co-display is the creation of a recombinant vaccine against *Pseudomonas aeruginosa* by insertion of a pilus-tip epitope of this bacterium in the S-layer protein RsaA [9]. Moreover, the manipulation of the S-layer might be useful to combat cancer. Immunization of wild type (WT) *C. crescentus* in a transplantable tumor prolonged survival and reduced tumor mass in a mouse model [10]. This

indicates that the S-layer could be used for more advanced applications to express toxic cargo or a ligand that targets the bacterium to tumor cells and initiate a localized immune response.

C. crescentus can also be used as a high level secretion system. Proteins can be fused with the carboxyterminal 336 amino acids of RsaA, which in many cases, results in secretion of large quantities of protein into the culture medium. The essential portion necessary for secretion is the last 82 aminoacids [11].

1.2 The structure of S-layers

1.2.1 Structural diversity but common problems among S-layers

S-layers are assembled from protein or glycoprotein subunits in a regular geometrical pattern. Different S-layers have different symmetries based on the number of protein monomers within a morphological unit: oblique (p1, p2), square (p4), or hexagonal (p3,p6) symmetry (**Figure 1**).

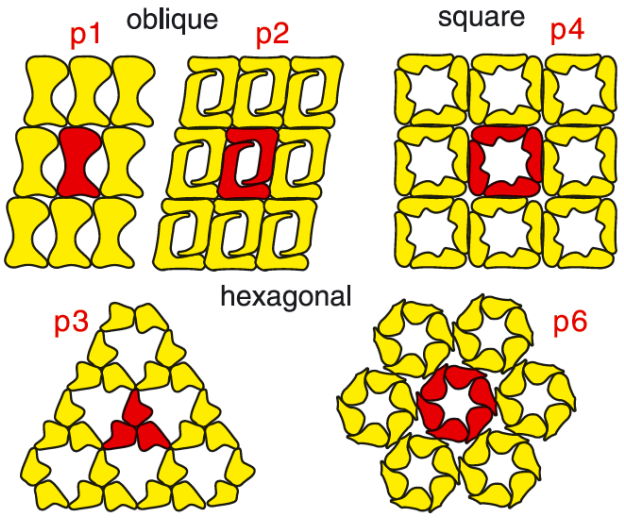

Figure 1. Possible S-layer lattices. S-layers exhibit a distinct geometric symmetry, depending on the number of monomers that constitute a morphological unit [1].

Depending on the organism, S-layers can consist of either a single protein or multiple proteins. The amino acid sequences of different S-layer proteins exhibit very low similarity. Detailed atomic resolution structures of lattices are not available but several low-resolution three-dimensional structures have been obtained by electron microscopy (EM) of negatively stained samples. The protein that assembles into an S-layer can be split up in a domain that

forms the main morphological unit of the lattice and a linker domain that connects individual protein monomers with each other. Together, this forms an organized network of proteins where pore diameters vary from 2-8 nm. S-layer proteins make up a substantial portion of the protein synthesized by the bacterial cell, spanning 7-31% of total protein production [12,13]. Determining the structure of S-layer proteins has been obstructed by the inherent property of S-layer monomers to spontaneously form a two-dimensional S-layer. Crystallization attempts of S-layer proteins for x-ray diffraction studies have therefore failed, as the protein aggregates during concentration. Interestingly, no three-dimensional protein-structure of atomic resolution exists for a full-length S-layer protein.

1.2.2 Towards a structure of the S-layer of *Caulobacter crescentus*

1.2.2.1 Current knowledge

Caulobacter crescentus is a Gram-negative, rod-shaped, dimorphic, oligotrophic non-pathogenic bacterium that can be found in soils and aquatic environments. It is completely covered by an S-layer that forms a hexagonal lattice. The S-layer is composed of about 40,000 identical 98 kDa protein monomers called RsaA. About 31% of protein synthesis of *C. crescentus* is dedicated to making RsaA [13]. RsaA is transported through the bacterial cell surface by a type I secretion system: An ATP binding protein (i.e. localized in the inner membrane) recognizes the non-cleavable C-terminal secretion signal of RsaA and transports it through the inner membrane by hydrolysis of ATP. Subsequently, RsaA traverses the periplasm through a membrane fusion protein. Finally, it is transported through the outer membrane protein [14]. Two outer membrane proteins are required for optimal secretion of RsaA [15]. Once outside, RsaA self-assembles into a hexagonal paracrystalline array. Initially, some RsaA monomers are anchored to a smooth lipopolysaccharide (SLPS) of the outer membrane by their N-terminus. Next, additional RsaA monomers interact with the anchored monomers, followed by interaction of monomers with those and so on. This results in a two dimensional extension into patches until the whole cell is covered [16].

Availability of a high-resolution S-layer structure would provide insights that would facilitate the exploitation of the application potential of the S-layer. When exogenous peptides are displayed in the S-layer, these inserts need to be positioned in a location where

protein folding and functionality are not compromised by adjacent RsaA proteins. The importance of insert-location has been demonstrated by a previous study in our lab. When multiple copies of the protein G IgG-binding domain were inserted combined with spacer sequences as opposed to only one copy, secretion efficiency and IgG binding affinity are much higher [6]. Accurate positioning of peptides is particularly important for displaying multimeric peptides or for the simultaneous display of an enzymatic pathway where the product of one enzyme is the substrate for another enzyme [17]. For this, knowledge of the three-dimensional structure of the S-layer at atomic resolution is essential. From a more fundamental point of view, having a three-dimensional structure would also greatly contribute to our understanding of S-layer secretion, anchoring and assembly. It has been shown that the first 225 amino acids of RsaA are necessary for anchoring to the outer membrane by interaction with SLPS [18]. However, the mechanism of anchoring is not understood. In addition, the structure could give information about Type I secretion of proteins. RsaA contains six Repeat in Toxin (RTX) motifs [19]. These motifs consist of a GGXGXDXXX consensus sequence and are known to bind calcium. Moreover, RTX motifs are present in all proteins secreted by a type I secretion system which indicates a functional role for the motifs in the secretion process [20]. A high-resolution structure could bring more clarity about this issue. Furthermore, it would shed light on the mechanism of assembly of the S-layer. In addition to manipulating S-layers on bacteria, it is of interest for nanotechnological applications to recrystallize the S-layer on other surfaces. This emphasizes the importance of understanding the assembly and anchoring process.

The highest resolution image obtained for the S-layer is at 2 nm (**Figure 2**). This was accomplished by negative stain electron microscopy and image reconstruction [21]. This structure shows that each hexagon is constructed out of 6 monomers. The pore diameter is ~2.5-3.5 nm, the distance between hexagon regions is 22 nm and the thickness is ~ 7 nm. Neighboring hexagons are connected by linker arms that originate from each monomer.

More recently, the primary sequence of RsaA has been correlated to certain positions within the hexagonal structure by site-specific nanogold-labeling experiments [2].This study showed that the N-terminus of RsaA forms the axis of three-fold symmetry that connects the hexamers within the layer, whereas the C-terminus is responsible for the axis of 6-fold symmetry as it builds up the hexamers (**Figure 2**).

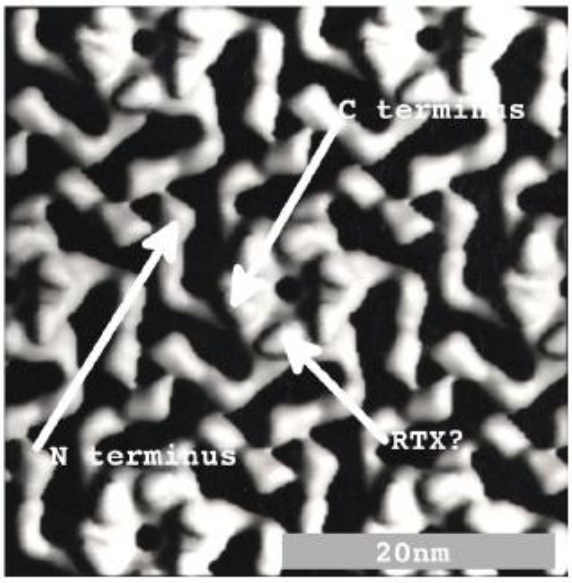

Figure 2. 3D reconstruction of the S-layer of *C. crescentus* shows a hexagonal array (resolution = 2 nm).
Each hexamer consists of 6 monomers and a linker arm emanates from each monomer to make connections with monomers from adjacent hexamers. White arrows show the location of the N-terminus and C-terminus [2].

As mentioned earlier, the determination of the structure at the atomic level by x-ray crystallization is impeded by the natural tendency of RsaA to undergo self-assembly into two-dimensional S-layer sheets, as three-dimensional crystals are needed. Other structure determination methods cannot be applied as RsaA is too big for NMR techniques. Neither are there proteins with sufficient homology, of which a structure is known. Thus comparative modeling techniques cannot be used. The S-layer protein of *Campylobacter fetus* showed the greatest similarity with RsaA (24% identity and 16.6% conservative substitution). Most of this similarity is due to the presence of RTX domains in both proteins, which are required for secretion. In my thesis I tackled the problem by using different approaches in parallel to produce crystallisable proteins; namely the use of truncated mutants, the use of nanobodies, disturbing an extremely hydrophobic region, screening S-layer mutants with RTX modifications and screening a library of S-layer mutants for S-layer shedding. X-ray diffraction experiments were performed in collaboration with Dr. Anson Chan (Murphy lab, University of British Columbia).

1.2.2.2 A truncated protein approach

It is possible that certain domains in the S-layer protein are responsible for aggregation, thus the protein would be more stable when these regions were genetically deleted. This impinges on studies performed on other S-layers, in which truncated forms of the protein were made and crystallized. This led to structures of the N-termini, (i.e. the attachment domain) of S-

layer proteins of the Gram-positive bacteria *Geobacillus stearothermophilus*, *Clostridium difficile* and *Bacillus anthracis* [22-24]. However, this does not yield knowledge for Gram-negative bacteria as the attachment mechanism is different in Gram-negative bacteria. More importantly, no structures exist of the core regions of S-layer proteins. Therefore, I chose to focus on the core region of RsaA, that is responsible for S-layer assembly. Indeed, in addition to using the full-length protein, I made and tested different N-terminal truncated mutants for improved protein behavior.

1.2.2.3 A nanobody aid approach

Nanobody-aided crystallization is a new method that has shown potential in the crystallization of some proteins [25-27]. A nanobody (Nb) is the recombinant antigen-binding domain of a camelid heavy chain antibody. Smaller than conventional antibodies; they can bind less accessible epitopes which makes them a valuable tool for structural biology. Nanobodies can assist crystallization by stabilizing a protein in a certain conformation. I employed nanobodies (Nbs) that bind to RsaA. The hypothesis was that a nanobody that can bind to one of the contact-points between RsaA subunits, thereby prevents assembly and aggregation. This would result in a monodisperse solution (i.e. contains only monomers). The initial experiments using Nbs were done in collaboration with Prof. Han Remaut (Structural and Molecular Microbiology, Vlaamse Universiteit Brussel).

1.2.2.4 Characterization of aggregation-inducing regions

The approach is based on the hypothesis that hydrophobic regions are involved in subunit-subunit interactions between RsaA monomers. Using TANGO, I was able to identify extremely hydrophobic regions in RsaA. TANGO is a computer algorithm that predicts aggregation nucleating regions in proteins as well as the effect of mutations and environmental conditions on the aggregation propensity of these regions [28]. The hypothesis is that substituting a core hydrophobic amino acid for a hydrophilic or charged amino acid would disturb the conformation of this region and thereby prevent subunit-subunit interactions. This would make the protein useful for crystallization trials if the overall folding remains intact.

1.2.2.5 Isolation of shedding mutants

Two clones, in which RTX regions were modified, were tested for shedding of protein and thus the potential lack of the capability to assemble into S-layers. In addition, two mutant libraries of *C. crescentus* with *Bam*HI sites or pilin epitopes inserted in the RsaA protein coding gene are available in the lab [11,29]. In mutants that shed RsaA, interactions between subunits might be disturbed by these small insertions.

1.2.3 Overall aim

The overall aim of this project was to devise methods to improve RsaA protein quality to enable crystallization of the protein. Crystallized protein would then be used in x-ray diffraction experiments in order to obtain a high-resolution structural model of the S-layer.

1.3 Functionality of S-layers

1.3.1 'Specific' versus 'specific and common' functions

The energy-consuming commitment to S-layer expression in a broad range of prokaryotes implies a pivotal role throughout evolution. It is probable that S-layers were primitive precursors prior to the acquirement of complex cell wall polymers. Due to their surface location and the fact that they completely cover the cell, S-layers have the potential to fulfill a broad spectrum of functions. Given long periods of time, they could have been modified to adopt different functions useful for the particular bacterium. In Archaea, it seems apparent that S-layers provide structural support, as most Archaea lack any other form of cell walls. The absence of spontaneous S-layer negative strains indicates their necessity. In some studied bacteria, certain functions can be assigned to structural domains in S-layers of specific bacteria (often pathogens in which these domains play roles in virulence). For pathogenic bacteria, S-layers have been shown to play a role in pathogenicity as they can act as protective coats, barriers against internal and external macromolecules or for cell adhesion and surface recognition. For example, the S-layer of *Campylobacter fetus* allows antigenic variability, which the bacterium uses to evade the immune response of the host. [30]. For environmental bacteria, it is often even less clear, what the advantage of having an S-layer is.

However, studies have shown that S-layers can offer protection against certain predators. S-layer positive strains of marine planktonic Cyanobacterium *Synechococcus* are protected against predation by the dinoflagellate *Oxyrrhis marina* compared to S-layer negative strains [31]. A similar phenomenon was observed for *C. crescentus*, *A. Salmonicida* and certain *Aquaspirillum* species. Some bacterial S-layers have also been shown to protect against predation by *Bdellovibrio* species (i.e. motile Gram-negative bacteria that predate other Gram-negative bacteria)[32]. More specifically, the presence of an S-layer offered *C. crescentus* protection from *Bdellovibrio exovorus*[33] . It has been assumed that S-layers form a mesh that excludes particles that are larger than its pore diameter and non-selectively allow free passage of small molecules such as nutrients and metabolites [34]. This so called 'molecular sieving' effect was studied in more detail in *B. staerothermophilus* [35]. Passive solute uptake was measured for solutes of various molecular weights. The result was that molecules up to 30,000 Da could freely traverse the S-layer, but exclusion limits were noted between 30,000 Da and 45,000 Da, which corresponds to exclusion of particles with a diameter of 4.5 nm or higher. In bacteria (including *C. crescentus*) S-layer pore diameters range from 2.5-3.5 nm. Larger channels are found in S-layers of some Archaea. Important to note is that these experiments were performed with S-layers recrystallized on sacculi prepared from whole cells, and therefore might not accurately represent natural situations, in which pore sizes might change depending on different environmental conditions.

Despite a list of observed and hypothesized functions for S-layers, a broad range of bacteria possess S-layers of which the function is still unknown. It is also possible that S-layers have evolved to take on different functions in different phylogenetic groups, where pore size and amino acid content (i.e. charged to neutral amino acid ratio) have adapted to the environmental conditions the bacteria reside in. However, the few studies that have been done to elucidate S-layer functions, took place in laboratory conditions and often only tested purified S-layers (interactions between S-layer and cell envelope are not included in this case) [36]. To represent reality more accurately, bacteria with fully assembled S-layers should be tested with regard to each factor that could mediate effects in their natural environments. One of the main problems in biology to date is to mimic natural environments in a controlled manner. An exhaustive list of every influential factor in the natural environment of a species is not available, due to the complexity present in nature. This results in a gap of information

regarding S-layer functionality. Overall, the occurrence of S-layers in a broad variety of phylogenetically distant prokaryotes, has made scientists assume, that no common function of S-layers is present. I argue that this is a premature conclusion, based on the absence of evidence. I suggest a common function shared by S-layers

1.3.2 Hypothesis: S-layer protects against cationic antibiotics

In this thesis, I propose and test the following hypothesis: S-layers have a protective role against small compounds that are harmful to the cell. In this study, the S-layer was studied for its protective effect against antibiotics, a group of small compounds harmful to cells. This is relevant because most bacteria encounter antibiotics in their natural environment. Environmental bacteria such as *C. crescentus* live in environments populated with a plethora of organisms (bacteria, plants, fungi), many of which produce antimicrobial compounds [37,38]. This could indicate that preservation of the S-layer through evolution was due to its role in bacterial survival. This idea was also supported by the fact that interaction by charges is possible so that S-layers could selectively prevent harmful compounds from reaching the cellular membrane. Most S-layers are acidic and interactions to trap cationic antimicrobials, such as antimicrobial peptides, could occur. This research was performed in collaboration with César de la Fuente-Núñez (Hancock lab).

1.3.3 Overall aim

The goal of this research is to investigate whether S-layers confer protection upon challenge with antimicrobials.

2. Materials and methods

2.1 Bacterial strains and growth conditions

The bacterial strains that were used are shown in **Table 1**. *E. coli* was grown in Luria-Bertani (LB) broth (1% tryptone, 0.5% yeast extract, 0.5% NaCl) at 37°C. *C. crescentus* was grown in PYE medium (0.2% peptone, 0.1% yeast extract, 0.01% $CaCl_2$, 0.02% $MgSO_4$) at 30 °C. For plates 1.3% agar was added. Transformations of *C. crescentus* and *E. coli* were done by electroporation [39]. The following antibiotic concentrations were used: chloramphenicol, 20 µg/mL for *E. coli* and 2 µg/mL for *C. crescentus*; ampicillin, 50 µg/ml for *E. coli*. Freezer stocks were made by mixing 50 µl dimethylsulfoxide (DMSO) and 950 µl of a broth culture.

Table 1. Bacterial strains and plasmids

Strain or plasmid	**Relevant characteristic(s)**	**Reference/Source**
Strains		
Caulobacter crescentus		
NA1000	Closely related to CB15, Ap^r, syn-1000, S-layer positive; holdfast defective; variant of wild-type strain CB15	[40]
JS1013	NA1000 with 353øB frameshift mutation (introduces amber codon at residue 358), S-layer-negative, holdfast defective	[18]
CB15	ATCC19089, wild-type strain, S-layer positive, holdfast positive	[41]
CB15ΔrsaA	CB15 with complete RsaA knockout, thus S-layer negative, holdfast positive	[42]
JS4026	CB2A (host strain similar to CB15), S-layer negative, holdfast negative, repBAC inserted into *xylX*	[13]
JS4032	CB2A (host strain similar to CB15), S-layer negative, holdfast negative, repBAC inserted into *xylX*, internal deletion of *ManB*	[13]
Escherichia coli		

Strain or plasmid	Relevant characteristic(s)	Reference/Source
DH5α	F-Φ80*LacZ*ΔM15(*lacZYA-argF*)U169 *recA1 endA1, gyrA96 thi-1 hsdR17 supE44 relA1 phoA*	invitrogen
Top10 F'	F-*mcrA Δ(mrr-hasRMS-mcrBC)* Φ80*lacZΔM15ΔlacX74 recA1 ara-D139Δ*(*araleu*) 7696 *galU galJ rpsL* (StrR) *endA1 nupG*	invitrogen
Plasmids		
pBSKII	Cloning vector; Ap^r	Stratagene
p4A	*E. coli* and *C. crescentus* shuttle vector; Cm^r	[18]
p4B	*E.coli-C.crescentus* shuttle vector; Cm^r	[13]
p4B:*RsaA600*	*RsaA* (with wild-type *rsaA* promotor) inserted into *Hin*dIII and *Eco*RI of p4B; Cm^r	[13]
p4B:*RsaAΔSD*	*RsaA* inserted after the modified *rsaA* promotor inserted as *Eco*RI-*Hind*III fragment; Cm^r	[13]
pTZ:*MtotI*	pTZ with *RsaA* with an internal deletion of T826-T892 and insertion of a pilin epitope; Cm^r	[29]
p4B:*Mtot1*	p4B with *RsaA* with an internal deletion of T826-T892 and insertion of a pilin epitope; Cm^r	This study
pTZ:*A19*	pTZ with RsaA; Cm^r	[11]
p4B:*A19*	p4B with RsaA; Cm^r	This study
p4B:*ΔEco*RV	p4B with *RsaA* with an internal deletion of D905-F907; Cm^r	This study
pUC cvx0.690ΦP (p336C)	Vector with *Eco*RI and *Hin*dIII restriction sites containing last 336 aa of RsaA; Cm^r	J. Nomellini, unpublished work.
p222	P336 where last 336 aa from RsaA are replaced by RsaA missing the first 222 aa; Cm^r	M. Ford, unpublished work
p892	P336 where last 336 aa from RsaA are replaced by RsaA missing the last 134 aa; Cm^r;	This study
p551	P336 where last 336 aa from RsaA are replaced by RsaA missing the first 551 aa; Cm^r;	This study
p4B:*Δ230-944*	p4B in which RsaA missing aa 230-944 is inserted; Cm^r	M. Jones, unpublished work

2.2 Plasmid and DNA manipulations

Standard methods were utilized [43] for all cloning procedures.

2.2.1 Construction of p4B:*A19*, p4B:*Mtot1*, p4B *ΔEco*RV

pTZ:*A19* carries full length *RsaA*. By using its flanking *Eco*RI and *Hin*DIII sites, the gene was moved to the multiple cloning site (MCS) of a p4B vector, creating p4B:*A19*. All manipulations were done in *E.coli* Top10 F'. This plasmid was brought into JS4026 and JS4032 through electroporation.

pTZ:*ΔEco*RV was constructed by making use of 2 *Eco*RV restriction sites at amino acid position 905 and 907 in *RsaA* of pTZ:*A19*. An internal fragment of 3 amino acids was deleted and the plasmid was subsequently religated. This resulted in the deletion of D905-F907. D905 is the last amino acid in the last RTX domain of RsaA and causes a subtle perturbation. The modified *RsaA* gene was moved to p4B by using its flanking *Eco*RI and *Hin*DIII sites, which created p4B:*ΔEco*RV. All manipulations were done in *E.coli* Top10 F'. This plasmid was brought into JS4026 and JS4032 through electroporation.

A more dramatic modification was made during the construction of ptz:*Mtot1* [29]. This plasmid contains RsaA under regulation of the modified *RsaA* promotor with an internal deletion of T826-T892 (i.e. 66 amino acid deletion with complete removal of the 4th and 5th RTX domain of RsaA), and an insertion at that site of a pilin peptide that is flanked by two *Bam*HI sites. The pilin peptide was cut out by using the *Bam*HI sites. The absence of the pilin peptide was confirmed by cutting with *Bcl*II (the pilin peptide contained this unique restriction site). This modified *RsaA* gene was removed from the vector by *Eco*RI and *Hin*DIII restriction and brought into the MCS of p4B, creating p4B:*Mtot1*. All manipulations were done in *E.coli* Top10 F'. This plasmid was brought into JS4026 and JS4032 through electroporation.

2.2.2 p222, p551, p892, p336 and p4B:*Δ230-944*

Cloning procedures described below were performed in *E.coli* Top10 F' and all clones were verified by sequencing.

p222, p336 and p4B:*Δ230-944* were previously made in the Smit lab and were brought into JS4032.

A pTZ vector with *RsaA* containing a *Bam*HI site at amino acid position 551 [29] was used. Truncated *RsaA* was transferred to the backbone of p336 using its flanking *Bam*HI and *Hind*III restriction sites, creating p551. This plasmid was brought into JS4032.

To create p892, the last 134 amino acids of *RsaA* were excised from ptz:*Mtot1*, using the *Bam*HI and *Hind*III restriction sites. This fragment was ligated into p336 (first the coding sequence for the last 336 amino acids was removed). p892 was brought into JS4032.

2.2.3 Site directed mutagenesis

A mutant was constructed in which valine 738 in *RsaA* is substituted for an aspartate, to disturb an extremely hydrophobic region. *E.coli* DH5α was used during the procedure. The clone was made by using site directed mutagenesis. Mutagenic PCR primers were designed and are listed in

Table 2. A 999 base pair fragment, covering the codon for residue 738, was excised from *RsaA* in p222, by using two flanking *Sac*II restriction sites. This fragment was ligated into pBSKII, which makes it a smaller plasmid to amplify. Selection for the insert was done by blue white screening. The plasmid was amplified, using the mutagenic primers. Subsequently, efforts were done to transfer the modified 999 base pair fragment back into the original backbone. Several methods (e.g. dephosphorylation backbone, manipulating the insert:backbone ratio, partial digests) were tried but failed.

Table 2. Mutagenic primers used for site directed mutagenesis.

Primer name	DNA sequence
RsaAGTC2212GAC_F	5'-CAACGTTGCGGTGAATGACGGCCTGACCGTTCTG-3'
RsaAGTC2212GAC_R	5'-CAGAACGGTCAGGCCGTCATTCACCGCAACGTTG-3'

2.2.4 Movement of libraries from pTZ to p4A

For the approach described in **1.2.2.5**, two mutant libraries (originally created with the help of the restriction enzymes *Aci*I and *Hin*PI of *C. crescentus*) were available in the lab, in which *Bam*H1 sites (introduces 4 amino acids) or pilin epitopes (introduces 26 amino acids) are inserted in the RsaA sequence [29]. With an *Eco*RI-*Hin*dIII digest, the library was moved to p4A (i.e. a generation 4 vector). These procedures were performed in *E. coli* Top10 F'. The libraries were transferred to the non-shedding strain JS4026.

2.3 Procedures for production and preparation of RsaA and truncates

JS4032 (i.e. an S-layer shedding strain) containing the proper expression plasmid was grown in test tubes with PYE and chloramphenicol at 30°C for 2 days. These cultures were used to inoculate 2.8 l fernbach flasks each filled with 100 mL PYE and chloramphenicol. These flasks were incubated at 30°C for 2 days with slow shaking (20 RPM) until an absorbance (600 nm) of 1 was measured for the cultures. Cell cultures were centrifuged at 8000 RPM and the supernatant was collected. The supernatant was transferred to lyophillization containers and frozen at -20°C. Subsequently, the supernatant was lyophilized (Freezone 2.5 Liter Benchtop Freeze Dry System, Labconco). Lyophilized protein with PYE components was collected and stored at -20°C. In the next step, a gel filtration column (Superdex 200 10/300 GL, GE Healthcare) was used to separate the PYE components and protein aggregates from soluble protein. First, 100 µg lyophilized product was dissolved per 2 mL of cold distilled water. The sample was centrifuged at 10000 RPM to remove cells and large protein aggregates, followed by a filtration step to remove smaller aggregates (0.22 µm Sterile Millex® Syringe Filters, Millipore). 500 µl of this sample was loaded onto the column. Because RsaA only contains a few tryptophanes, it was difficult to observe by a UV detector at 280 nm. Therefore the protein sample was visualized by measuring absorbance of peptide bonds at 205 nm. $RsaA_{\Delta 0\text{-}222}$ fractions collected from the column had an average concentration of 2 mg/mL. The truncated $RsaA_{\Delta 0\text{-}222}$ was concentrated using aquacide II (EMD). This is a sodium salt of carboxymethylcellulose with an extremely high viscosity.

After concentration measurements (see **II.4**.), the protein was added to a dialysis bag (Spectra/Por Dialysis Membrane, MWCO: 6-8,000). The dialysis tubing was kept wet and completely covered with aquacide II. Protein samples of 10 mL or less could be concentrated to 2 mL or less within an hour. After concentrating, the samples were filtered again (0.22 µm Sterile Millex® Syringe Filters, Millipore). When a detergent was used in an effort to enhance solubilization of protein (0.1% LDAO, 0.1% octyl glucoside, 0.1% CHAPS), these were added before concentrating. Proteins were also checked at different steps of the process by SDS-PAGE (**2.8**).

2.4 Protein concentration determination

The Micro BCA protein assay kit (Pierce) was used for assessing protein concentrations according to their protocols. A bovine serum albumin (BSA) standard curve was set up to determine nanobody concentrations. Because of the deviating amino acid content of RsaA compared to BSA, different standard curves were used. A standard curve representing full length RsaA was used for estimation of concentrations [13]. Protein samples were filtered before measurements (0.22 µm Sterile Millex® Syringe Filters, Millipore) to remove impurities.

2.5 Monodispersity tests

To assess protein behavior and thus suitability for crystallization, dynamic light scattering (DLS) was utilized (Dynapro™ Plate Reader, Wyatt Technology Corporation). This tool measures the polydispersity level of a protein sample and estimates the hydrodynamic radius of the particles in the solution, as well as the molecular weight. For measurements, 70 µL protein sample was placed in one of the wells of a 384-well black plastic plate with a glass bottom (Sensoplate, Greiner Bio-One). To remove air bubbles, the plate was centrifuged for 2 min at 2000 RPM. Data was analyzed by Dynamics 7 software. The Dynapro™ Plate Reader also allowed one to design experiments to increase temperature with time. This was done to set up a temperature profile for both RsaA truncations: Δ0-222 and Δ0-551. The machine was cooled with liquid nitrogen to allow measurement at temperatures lower than

RT. Measurements were recorded at increments of 2°C, starting from 4°C and ending at 48°C.

2.6 Crystal screens and seeding efforts

Well-behaved protein samples that were sufficiently concentrated were utilized in a variety of crystal prescreens. Sitting drop crystal screens were set up using 384 unique screening conditions of the (JCSG Core Suites I, II, III, IV; Qiagen). These screens contain the commercially available conditions that gave experimentally the highest hit rates. 96 well plates (Intelli-plate® 96 low volume reservoir, Art Robbins Instruments), that contain two wells for drops, were used. 90 µL of each condition was added per reservoir. The 2 wells were used to test different drop:condition ratios (1 µL:1 µL and 2 µL:1 µL were tested), to compare different protein concentrations or to test for differences when calcium acetetate was added. Crystal formation was observed by polarized light microscopy.

Based upon observations of the prescreens, hanging drop screens were designed. This allows the use of bigger drops (thus more protein available for crystallization). 24 well plates (VDX plate with sealant, Hampton Research) and glass cover slips (Fisher Scientific) that were silanized, were used. Stock solutions of different precipitants, buffers, filtered distilled water and other additives were made. Subsequently, they would be mixed so that desired concentrations were established in a total volume of 500 µL. This was added to the well reservoir. Silanized cover slips were washed with ethanol before use. Then a drop of protein sample would be placed to which a drop of condition was added. Drop:condition ratios that were used were: 4 µL:2 µL and 6 µL:3 µL. A range of buffers and precipitants were tested. Screens were initially stored at RT, but in most later experiments at 4°C, for protein stability purposes.

Seeding efforts were done, in order to try to increase crystal size. Micro-seeding was done by crushing existing crystals using a cat whisker and transferring them to a new drop with the same conditions in which the initial crystals grew, but with fresh protein sample. To decrease the number of crystal nuclei, the same cat whisker was swept to several more drops that contained the same conditions. Macro-seeding was done similarly, but a complete crystal was now transferred to a drop with identical conditions.

2.7 X-ray diffraction

Protein crystals were placed in a drop of its reservoir solution. To this, cryoprotectant was added (i.e. 30% glycerol, or 25% ethylene glycol). Next, the protein crystals were mounted with a cryoloop (Mounted CryoLoop^{TM}, 0.005-0.1 mm, Hampton Research). As x-ray source was opted for the MicroMax^{TM} 007 HF (Rigaku) with a CCD detector (Saturn 944 HG, Rigaku). The loop was placed on the goniometer and the crystal was instantly frozen by a liquid nitrogen stream. The x-ray beam was shot through the sample from different angles, to find the best diffraction. Diffraction patterns were collected with the HKL 3000 software (HKL Research inc.).

2.8 SDS-PAGE, western blot and low pH extraction

SDS-PAGE was performed using 12% and 13% separating gels. The gels were stained with Coomassie Brilliant Blue R-250. Western blots were done using standard methods [43]. Low pH extraction of S-layer protein was done as described previously [44].

2.9 Initial nanobody construction procedures

J. Nomellini prepared an RsaA sample using the low pH extraction method [16], after which it was concentrated using Amicon Ultra centrifugal filter units (3,000 MWCO, Millipore). Eliciting of and selection for RsaA-binding Nbs was done at the lab of Professor Han Remaut (Structural and Molecular Microbiology, Vlaamse Universiteit Brussel). Llamas were injected with the RsaA sample to raise heavy-chain antibodies against RsaA. Peripheral blood lymphocytes were isolated, from which total RNA was extracted. cDNA was synthesized and one pair of primers was used to amplify the complete nanobody repertoire. To identify the 10 best binding nanobodies, the nanobody repertoire was cloned into a phage display library. The nanobody sequences were inserted in a pHEN6 vector for expression in the periplasm of *E.coli* (WK6) as C-terminal His_6-tagged proteins. Colonies that were selected by panning were screened by ELISA (enzyme-linked immunosorbent assay). Detailed procedures were described previously [45]. **Figure 3** shows the alignment of the amino acids of all 10 Nbs.

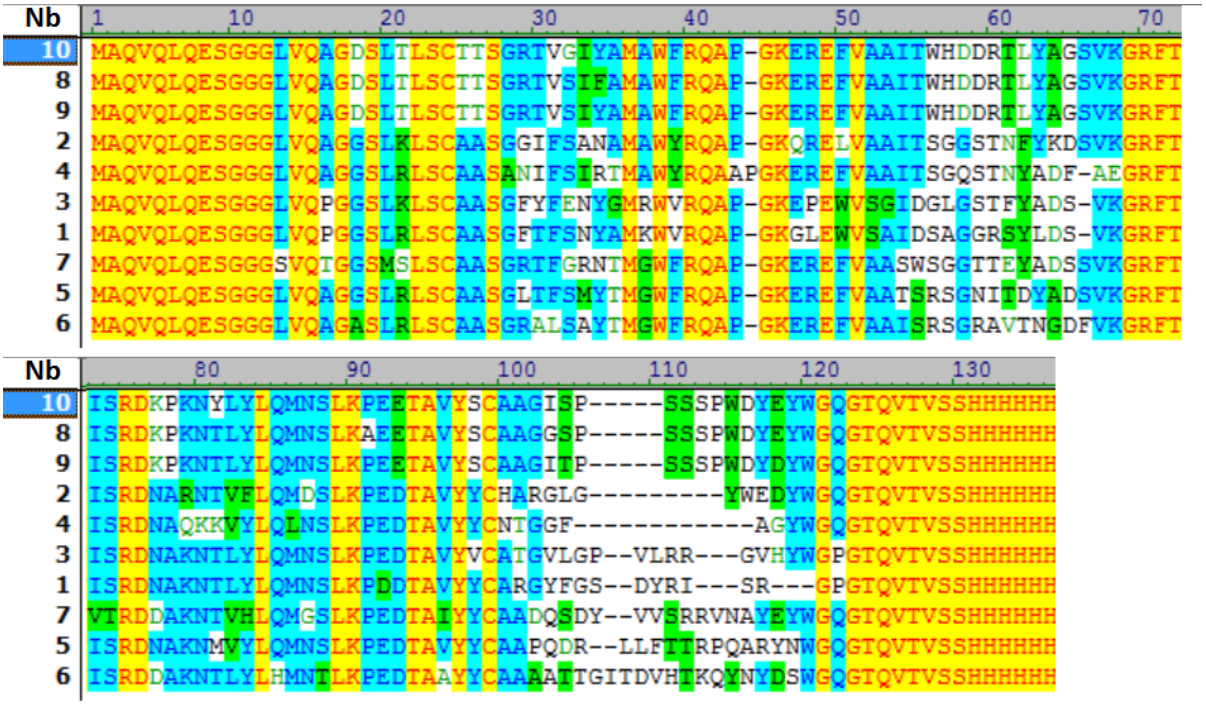

Figure 3. Amino acid alignment of 10 Nbs that bind RsaA.

2.10 Nanobody expression, extraction and purification:

The nanobody expressing cells were grown overnight at 37°C in LB supplemented with ampicillin, in a shaking incubator. When an absorbance of 1 was measured, 10 ml of cells was added to 1 L LB (plus ampicillin). Flasks were shaked at 37°C. Because the nanobody yield is low, 6 L culture was grown simultaneously. When the bacteria reached their exponential growth phase (OD 0.7-0.8), cells were induced by addition of 1 ml 1M IPTG (isopropyl β-D-1-thiogalactopyranoside) to each flask, and would be shaked for an additional 3 hours at 37°C. Nanobodies were extracted from the peripasmic space according to the following protocol. The bacterial cultures were centrifuged for 15 minutes at 6000 RPM (4°C). The supernatant was decanted, and the cell pellet was suspended in 20% sucrose with 20 mM Tris pH 8.0 (4 mL/g wet cells). To further destabilize and remove the outer membrane 40 µL 0.5M EDTA and 40 µL lysozyme (10 mg/mL) were added per gram of wet cells. This mixture was kept on ice for 20 minutes, followed by a centrifuging for 20 min at 12000 RPM (4°C). The supernatant, which contained the nanobodies was collected and the remaining cell debris was disposed of. The periplasmic extract still contained other components from the outer membrane and the periplasm, hence a purification of the

nanobody was required. Therefore, the C-terminally fused HIS_6-tag of the nanobody was used for purification by immobilized metal ion chromatography (IMAC) using a HIS-TRAP™ column (GE Healthcare, high performance, 5ml, Ni-sepharose). First, the EDTA in the extract was neutralized with 80 µL $MgCl_2$ (1M) in order to prevent stripping of nickel ions from the column. Washing buffer (20 mM Tris pH 8.5, 250 mM NaCl, 5 mM Imidazole, in distilled water) and elution buffer (20 mM Tris pH 8.5, 250 mM NaCl, 500 mM Imidazole, in distilled water) were prepared. An ÄKTAexplorer™ (GE Healthcare) was used to run all volumes and detect when Nbs where eluted. The column was washed with 5-10 CV (column volume) distilled water, followed by 5-10 CV washing buffer (at 4 mL/min). Subsequently, the periplasmic extract was loaded onto the column with a 25 ml syringe and was run at 1 ml/min. Next, 5-10 CV washing buffer were run over the column (5 mM imidazole removes contaminating protein from the column). Next, a gradient in which the concentration of elution buffer gradually increases was started. The nanobodies eluted in a concentration range of 200-250 mM imidazole. The purified nanobodies were dialyzed overnight at 4°C in 25 mM Tris (Spectra/Por®Dialysis Membrane MWCO: 6-8,000), to remove the imidazole. Nanobody concentrations were determined (see **2.4.**) and were checked on 13% SDS-PAGE gels (see **2.8.**). They were concentrated with Amicon Ultra centrifugal filter units (3,000 MWCO, Millipore) to approximately 1 mg/mL. Final concentrations were confirmed by measurement and SDS-PAGE (see **2.4.** & **2.8.**). Concentrated nanobodies were stored at -80°C.

2.11 Nanobody-RsaA binding assays

2.11.1 Whole cell labeling with nanobodies

50 µL of JS4026 (OD 1) was centrifuged for 3 min at 13000 rpm. Cell pellets were suspended in 100 µL cold PYE. 15 µL of periplasmic extract (containing Nb) was added and incubated on ice for 15 min. Cells were washed with PYE and a Rabbit his-probe (G18, Santa Cruz Biotechnology, inc.)was added (1:100 dilution) and the mixture was incubated for 30 min on ice. The cells were washed again followed by the addition of secondary antibody (i.e. goat anti-rabbit conjugated with Alexa Fluor® 488, invitrogen) (1:200 dilution). Cells were subsequently washed 3 more times with PYE and were dissolved in 20 mM

phosphate buffer with 50% glycerol and 2% n-propyl gallate. The cells were examined using epifluorescence microscopy.

2.11.2 Spot blots

10 µL of RsaA was added on a PVDF membrane and was allowed to dry for 30 min, after which it was incubated in blocking buffer for 30 min. Then, 15 µL Nb extract was added to 10 mL of blocking buffer. The membrane was incubated for 30 min, followed by a washing step. A Rabbit his-probe (G18, Santa Cruz Biotechnology, inc.) was added in a 1:500 dilution and the membranes were incubated for 30 min after which they were washed. Then, Secondary goat anti-rabbit antibody conjugated with HRP (horse radish peroxidase; 1:250 dilution) was added. The membrane was incubated for 45 min, with shaking. Subsequently, the membrane was washed with blocking buffer, followed by a washing step with TBS (Tris Buffered Saline). The colorimetric detection was performed by adding detection reagent (i.e. 5 ml methanol, 15 mg 1-chloro-1 naphtol, 20 ml TBS and 50 µl H_2O_2).

2.11.3 Western blot development

Western blots were performed as in **2.8.** A triple labeling procedure was done. First 15 µL of Nb extract was mixed in 10 ml blotto. Membranes were incubated for 1h and subsequently washed. Rabbit his-probe (G18, Santa Cruz Biotechnology, inc.) was added in a 1:1000 dilution and the membranes were incubated for 1h. After washing, goat anti-rabbit antibody conjugated with Alexa Fluor®680 (invitrogen) was added in 1:10000 dilution. Membranes were washed and scanned by an infrared scanner (Odyssey Infrared Imager, LI-COR).

2.12 Isolation and assessment of nanobody-RsaA complex

The periplasmic Nb extract was incubated with RsaA samples that had been purified as described in **2.3**. The M_w of a nanobody is ~ 15 kDa, whereas the M_W of $RsaA_{\Delta 0\text{-}222}$ is ~ 75 kDa. For each $RsaA_{\Delta 0\text{-}222}$ molecule to bind a Nb, 400 mL Nb (1 mg/mL) has to be added to 2 mL $RsaA_{\Delta 0\text{-}222}$ (1 mg/mL). This mixture was incubated at 4°C for 2 hours, after which it was purified on a HIS-TRAP™ (GE Healthcare, high performance, 5ml, Ni-sepharose) column as described in **2.10**. Isolated Nb-$RsaA_{\Delta 0\text{-}222}$ was assessed by DLS.

2.13 Colony western assays

JS4026 cells containing the library were grown on PYE agar (with chloramphenicol). After 2-3 days, colonies appeared. A colony was picked with a pipet tip and dissolved in 100 µL cold PYE. 1.5 µL of this suspension was placed as a drop on a fresh PYE agar plate (no selection marker). For each tested clone a drop was placed on this plate, after which it was placed in a 30°C incubator. 2-3 days later, a PVDF membrane was laid over the agar for 30 min. The membrane was removed and incubated in blocking buffer for another 30 min, while shaking. The membrane was flipped over, followed by 20 min of shaking. Next, the membrane was incubated with a primary polyclonal rabbit anti-RsaA antibody (1:1000 dilution) for 1 hour. Two washing steps with blocking buffer were performed. Then, Secondary goat anti-rabbit antibody conjugated with HRP (horse radish peroxidase; 1:250 dilution) was added. The membrane was incubated for 45 min, while shaking. Subsequently, the membrane was washed with blocking buffer, followed by washing step with TBS (Tris Buffered Saline). The colorimetric detection was performed by adding detection reagent (i.e. 5 ml methanol, 15 mg 1-chloro-1 naphtol, 20 ml TBS and 50 µl H_2O_2). As a control for these assays, strains JS4026 and JS4032 with p4BA19 were used.

2.14 MIC assays

In the first experiments, JS4026 and JS4026, complemented with p4B *RsaA600* were used as S-layer negative and S-layer positive strain respectively. Test tubes with 5 ml PYE were inoculated with each strain and grown at 30°C with shaking in a rotating wheel. After 24 hours, absorbances were measured and both strains were diluted to an OD of 1.05. Ceftazidime, tetracyline, ciprofloxacin and the peptides 1018, 1037 and LL37 (GenScript, synthesized chemically by Fmox chemistry) were weighed and dissolved in water to obtain a range of concentrations. Later on, the isogenic S-layer positive strain NA1000 and S-layer negative strain JS1013 (has a frame shift mutation in *RsaA* making it null) were subjected to an expanded assortment of peptides. The assay is based on broth microdilution methods described previously [46]. Polypropylene 96-well plates with clear round bottoms (Corning®) were used. Subsequently these cultures were diluted 100x with PYE. In each well, 5 µL antibiotic and 95 µL bacterial cells were mixed. As a control 5 µL water instead of antibiotic

was used. This was done for both strains at each of the different concentrations and replicated in 8 wells. Next, the plate was incubated for 24 hours at 30°C. After 24 hours optical densities (600 nm) were measured.

2.15 Killing assays

NA1000 and JS1013 were treated with one concentration of LP1 or LL37, using the 96-well plates as described in section **2.14**. At different time points, cells were collected (3 different wells) of which serial dilutions were made. These different dilutions were plated on PYE agar plates and incubated at 30°C. After 2 days, CFUs (colony forming unit) were counted.

2.16 Growth curves

NA1000 and JS1013 were treated with LL37 as described in section **2.14**, but volumes in the 96-well plates were doubled (i.e. 10 µL LL37 and 190 µL cells in PYE). OD_{620} values were measured every 20 minutes over a time period of 25 hours (TECAN Spectrafluor Plus plate reader)

2.17 Biofilm assay

The biofilm-forming strains CB15 (s-layer positive) and CB15ΔrsaA (s-layer negative) in which the holdfast (necessary for biofilm formation) is not knocked out, were treated with increasing concentrations of LP1 and LL37 as follows**.** Test tubes with 5 ml PYE were inoculated with each strain and grown at 30°C with shaking in a rotating wheel. After 24 hours, optical densities were measured and both strains were diluted to an OD of 1.05. Subsequently these cultures were diluted 100x with PYE. Polypropylene 96-well plates with clear round bottoms (Corning®) were used. In each well, 5 µL peptide and 95 µL bacterial cells were mixed. As a control 5 µL water instead of antibiotic was used. This was done for both strains at each of the different concentrations and replicated in 8 wells. Next, the plate was incubated for 24 hours at 30°C. The plates were washed and biofilm formation was quantified by staining adhered cells with crystal violet and recording absorbance levels at 595 nm [47].

2.18 Supplementation assay

An attachment negative strain (JS4032) with p4B:*rsaA600* was grown in M15 minimal medium [13] at 30°C with shaking. When an optical density of 1 was measured, the cells were pelleted and the supernatant was collected. Next, the supernatant was dialyzed (using Spectra/Por®Dialysis Membrane MWCO: 6-8,000) in water overnight. The presence and purity of the protein was confirmed before and after dialysis by SDS-PAGE. Next, the supernatant was lyophilized. The lyophilized protein was dissolved in water to concentrations for use in the supplementation assay. A modified protocol for the broth microdilution method was used: JS1013 was treated with increasing concentrations of RsaA and one single concentration of LL37 (MIC for JS1013). After 24 hours, optical densities (600 nm) were measured.

2.19 Double fluorescent labeling

Strains NA1000 and JS1013 were treated with biotinlylated LL37 (B-LL37) for 30 minutes using the 96-well plate assay (see **2.14**.). Subsequently, the cells were washed with 0.25X PBS and incubated on ice for 30 min with (1:200 dilution) streptavidin Alexa Fluor® 488 conjugate (invitrogen, green label) to label B-LL37. The S-layer was visualized by incubating the cells for 30 min with polyclonal rabbit anti-RsaA antibody (1:200 dilution). After washing, a goat anti-rabbit antibody conjugated with Alexa Fluor® 568 (invitrogen, red-orange label) was added to the cells (1:200 dilution), followed by a waiting period of 30 min. After 3 more washing steps, the cells were centrifuged and dissolved in 20 mM phosphate buffer with 50% glycerol and 2% n-propyl gallate. They were studied using phase contrast and epifluorescence microscopy.

2.20 Statistical and graphical analyses

Data of the protection assay experiments were statistically analyzed for significant differences between S-layer positive and S-layer negative strains at different concentrations. For each peptide, datasets were analyzed as follows. First the background signal (i.e. the average OD_{600} measured in wells filled with PYE) was subtracted from each value. These values were normalized by dividing them by the average value that was measured for their

respective controls (i.e. no antibiotic treatment), after which they were transformed into percentages. Based upon this, the mean percentage was calculated per dose for both strains. Each value represent the % survival after treatment. All calculations were performed in Microsoft Excel.

On this data, a 2-way ANOVA analysis was performed to investigate whether interaction was present between 2 variables: X: presence of S-layer and Y: antibiotic dose. Significance levels were given by P-values. When interaction between the 2 variables was observed (i.e. P-value < 0.05), pair wise comparisons were done between S-layer negative and S-layer positive strains to assess at which doses, differences in survival are significant, after Bonferroni correction for multiple testing. GraphPad Prism 5 software was used for all the statistical analyses.

In order to graphically represent the protective effect against antibiotics by the presence of S-layers, the survival percentage values were further transformed in Microsoft Excel. Each value for the S-layer negative strain was subtracted from the corresponding value for the S-layer positive strain. The % protection at each of the 5 antibiotic doses was visualized with bar graphs, in which each bar is accompanied with its error bar and significance level.

3. S-layer proteins: control of monodispersity and crystallization

3.1 Novel methods achieve high quality concentrated RsaA

Through trial and error, a new method was created to produce well-behaved (i.e. monodisperse) protein (**Figure 4**). It was essential to use tools that aim on minimizing protein agitation. Full-length protein could not be prepared with this method (or any previously tested method). When protein was concentrated by suspending lyophilized full-length protein, nearly all of it formed high- or low-molecular weight aggregates. The first was excluded by centrifugation whether the latter was removed in the filtering step. Therefore, N-terminal truncation mutants were made and tested: $RsaA_{\Delta 0\text{-}222}$, $RsaA_{\Delta 0\text{-}551}$ and $RsaA_{\Delta 0\text{-}690}$. Using aquacide, $RsaA_{\Delta 0\text{-}222}$ could be concentrated up to 4 mg/mL. Any attempts to increase the concentration, failed. $RsaA_{\Delta 0\text{-}551}$ proved to be more difficult to concentrate as its maximum concentration was ~ 2 mg/mL. Protein quality was assessed by measuring polydispersity by DLS. $RsaA_{\Delta 0\text{-}222}$ (4 mg/mL) behaved as a monodisperse mixture. The polydispersity recorded was 23.2% and the calculated hydrodynamic radius was 4.3 nm (**Figure 5B**). $RsaA_{\mathbf{\Delta 0\text{-}551}}$ (2 mg/mL) showed in one case a polydispersity of 18.3 with a R_h of 5.3 nm (**Figure 5A**). However, $RsaA_{\Delta 0\text{-}551}$ showed a lot of variability in Rh and poydispersity measurements between different preparations, ranging from 3-12 nm and 18-50% respectively. This was similar to results obtained with the smaller $RsaA_{\Delta 0\text{-}690}$. Hence, this truncate was omitted from further studies. $RsaA_{\Delta 0\text{-}222}$ samples consistently showed R_h between 4 and 4.5 nm. Polydispersity values varied but were never higher than 25% at concentrations of 4 mg/mL or lower. Further, to compare protein stability for both truncates, a DLS temperature profile was made. Polydispersity values were recorded at each increment of 2°C, starting at 4°C and ending with 48°C (**Figure 6**). $RsaA_{\Delta 0\text{-}551}$ appeared to be very unstable when temperatures were higher than 10°C. Around RT, nearly half of the protein content had formed aggregates. $RsaA_{\Delta 0\text{-}222}$ was monodisperse between 4°C and RT. Even at 48°C, only 20% of the protein had formed aggregates. These experiments all highlight that $RsaA_{\Delta 0\text{-}222}$ is much more stable than $RsaA_{\Delta 0\text{-}551}$. Therefore $RsaA_{\Delta 0\text{-}222}$ was used for further experiments. Different buffers and additives were also assessed for improvements, using

DLS (**Table 3**). None of these changes however improved polydispersity values over the initial solvent choice (i.e. 25 mM NaCl and 5 mM Tris pH 7.5).

To surpass the concentration limit of 4 mg/mL, different neutrally charged detergents were added to the samples during the concentration process: CHAPS, LDAO and octyl glucoside. LDAO and octyl glucoside allowed higher concentrations, but polydispersities were higher than 50%. In contrast, 0.1% CHAPS (i.e. a zwitterionic detergent) had a favorable effect; protein could now be concentrated up to 7 mg/mL without significant losses in monodispersity (**Figure 5C**). With this new knowledge, polydispersities were measured for concentrations higher than 4 mg/mL of $RsaA_{\Delta 0\text{-}222}$ with 0.1% CHAPS (**Figure 7**). The protein samples could not be concentrated at higher levels than 9 mg/mL.

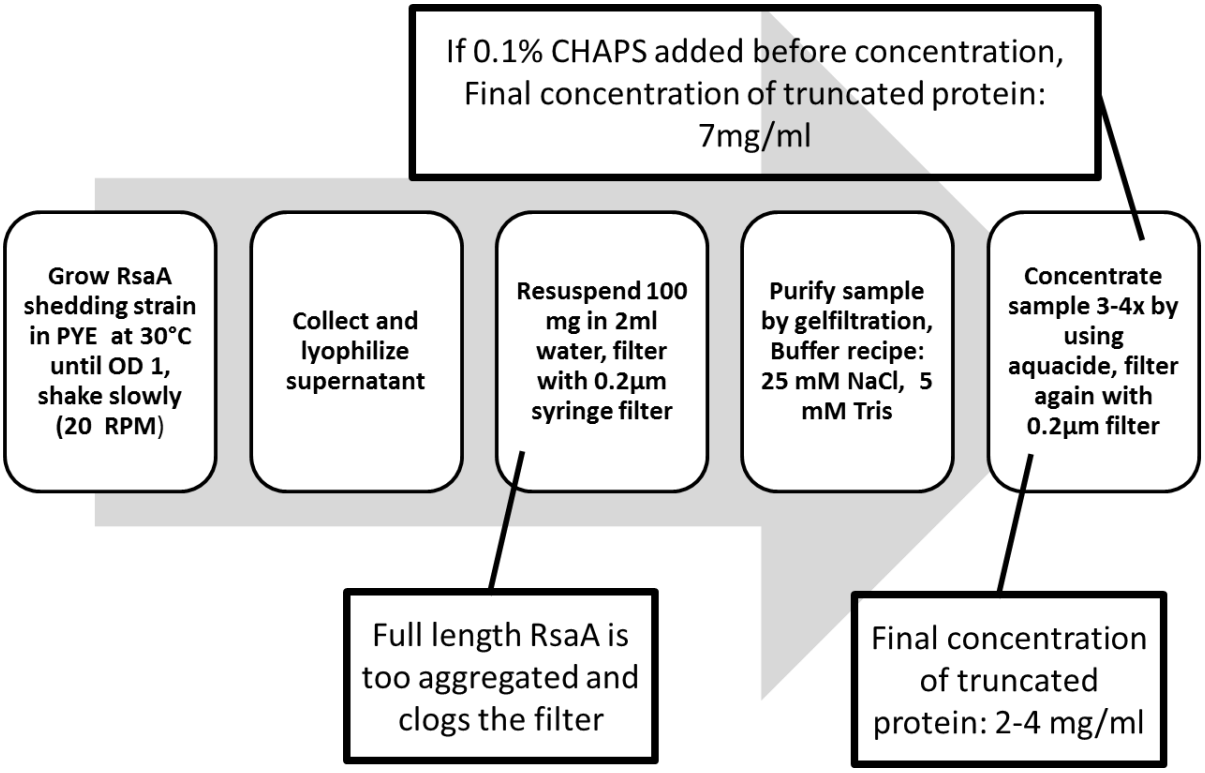

Figure 4. Flow chart designating the steps to make monodisperse RsaA protein samples.

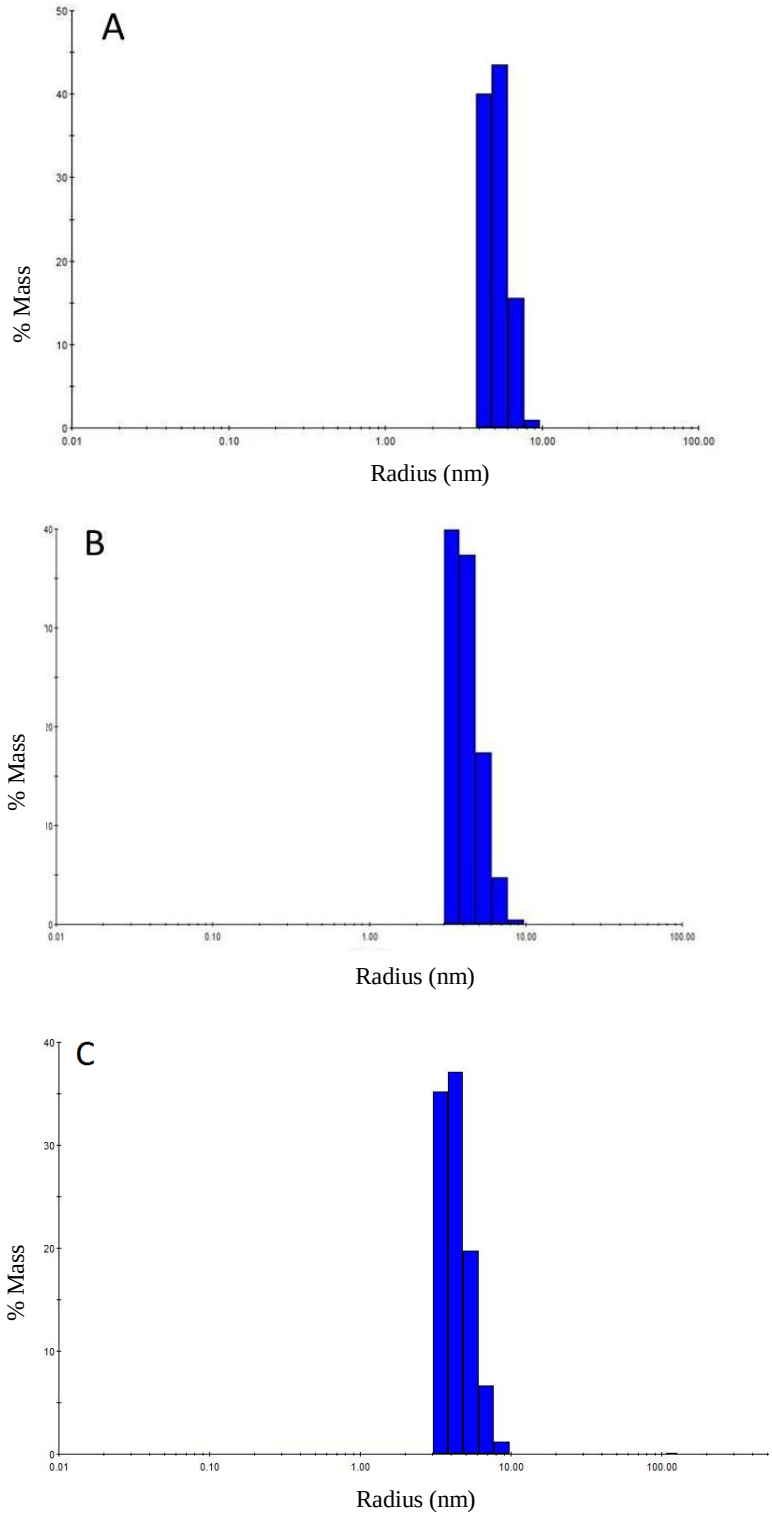

Figure 5. Dynamic light scattering measurements of RsaA truncation mutants
A) $RsaA_{\Delta 0\text{-}551}$: concentration = 2 mg/mL, % polydispersity = 18.3, Radius = 5.3 nm B) $RsaA_{\Delta 0\text{-}222}$: concentration = 4 mg/mL, % polydispersity = 23.2, Radius = 4.3 nm. C) $RsaA_{\Delta 0\text{-}222}$ and 0.1% CHAPS: concentration = 7 mg/mL, % polydispersity = 25, Radius = 4.4 nm.

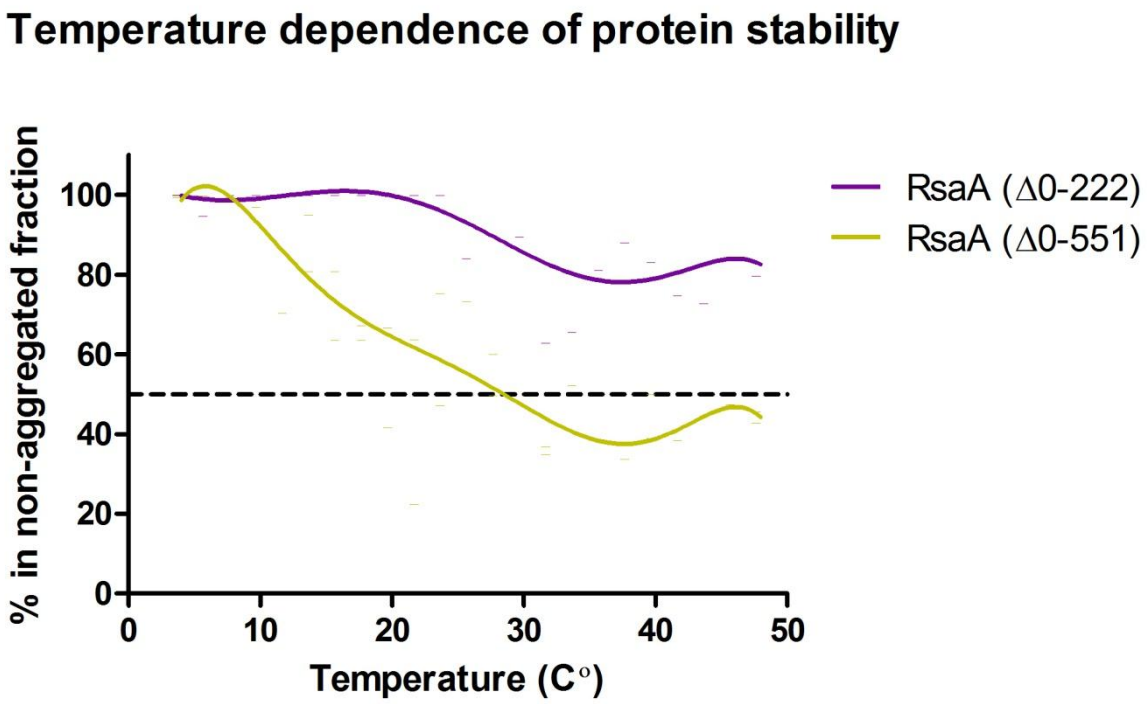

Figure 6. Temperature profile for the truncation mutant Δ0-551 (1 mg/mL) and Δ0-222 (4 mg/mL). Two samples from different protein batches were tested. The Y-axis shows how much protein is soluble at a given temperature. When temperature increases, more soluble protein will aggregate. The propensity to aggregate is much higher for RsaA $_{\Delta 0\text{-}551}$ than for RsaA $_{\Delta 0\text{-}222}$ even though the latter sample was 4 times more concentrated. Datapoints represent the average of two values.

Table 3. Precrystallization buffer/additives screen*

Buffer or additive	% Polydispersity
50 mM NaCl pH 9	27.9
500 mM Trehalose pH 9	43.5
25 mM MOPS pH 7	44.1
25 mM TES pH 7.5	35.1
50 mM arginine pH 9	45.1
500 mM arginine pH 9	36.5
7.5 mM triethanolamine pH 8	33.2
2.5 mM EDTA pH 9	47.6
10 mM PEG	22
25 mM Glycine	27.2

*several buffers/additives were added to a monodisperse RsaA$_{\Delta 0\text{-}222}$ sample (2 mg/mL; in 25 mM NaCl and 5 mM Tris pH 7.5; polydispersity = 15.5%) and polydispersities were measured using DLS.

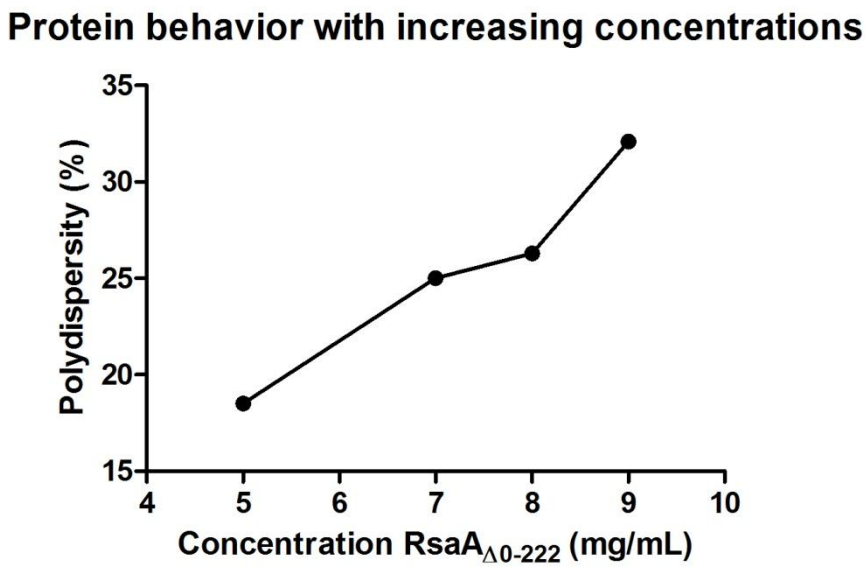

Figure 7. Relationship between protein concentration and polydispersity.
A semi-linear increase in polydispersity with increasing protein concentration is present. The upper concentration limit is 9 mg/mL. RsaA$_{\Delta 0\text{-}222}$ was solubilized with 0.1% CHAPS.

3.2 Crystallization trials show that S-layer proteins crystalise

The monodisperse RsaA$_{\Delta 0\text{-}222}$ samples were used to set up precrystallization screens using the JCSG core I, II, III and IV crystallization screens and the sitting drop method. These screens showed that crystallization occurred after 2 weeks in the presence of 200 mM Calcium acetate, 20% w/v PEG8000 and 0.1M MES pH6. In the absence of calcium, no crystals could be formed. In addition, it was noted that using a sample:condition ratio of 2:1 improved crystal formation over a ratio of 1:1. Because of the higher stability at lower temperature, the plates were incubated at 4°C.

Based upon these results, additional crystal screens were designed and set up, using the hanging drop method, which allowed the use of higher sample amounts. Starting from the optimal condition observed in the JCSG screens, different variations were tested. pH ranges were explored by varying the conditions. Several buffers (MES, Tris, CHES, MOPS, HEPES) with pHs between 5.5 and 9.5 were used. No significant changes in crystal formation were seen due to varying pHs. Furthermore, PEGs of different molecular weight were interchanged: PEG2000, PEG3350, PEG4000, PEG6000 and PEG8000. Interestingly, crystals could only form in the presence of PEG8000. Afterwards, percentages of PEGs were

also increased as well as lowered, ranging from 18-25%. In this range, no improvement of crystal formation was visible. Different calcium acetate and $CaCl_2$ concentrations were tested as a source of Ca^{2+} ions with concentrations ranging from 5 mM to 300 mM. Furthermore, increasing the amount of NaCl up to 200 mM appeared to prevent crystallization. In order to provide more protein for the crystallization process, sample: condition ratios were increased to 4:2. This led to the formation of more crystals. Augmentations to 6:3, slowed the crystallization process dramatically and did not improve crystal quality. Optimal results were obtained under the following conditions: 20% w/v PEG8000, 200 mM Calcium acetate and 0.1M MES pH 6 (**Figure 8**). The crystals were very thin sheets and hence required further optimization.

Another divalent cation, strontium, was used to investigate if it could substitute for calcium. 200 mM $SrCl_2$ (in combination with 20% w/v PEG8000 and 0.1M Tris pH7.5) formed thicker crystal sheets after 5 weeks (**Figure 9**). A range of varying conditions was used to come to this conclusion. $SrCl_2$ was added in different concentrations ranging from 5-200 mM. Several different buffers with different pH values were tested, but led to similar results as before. The amount of PEG8000 was also varied between 0-40%, but optimal results were accomplished in the range of 20%. As from 30% PEG8000, crystals formed sooner but in the shape of needles and more protein precipitation was observed. In order to try to increase crystal size, both crystals formed in the presence of calcium and strontium were used for seeding, using micro- and macro-seeding techniques. However, in the most positive case, this led to formation of crystals of comparable size to the original crystals. Crystal screens were also set up for highly concentrated $RsaA_{\Delta 0\text{-}222}$ samples with CHAPS. Using Strontium, thicker crystals were established than by all previous methods (**Figure 10**). These crystals were also more clustered with each other. Screens were also set up to see if a collection of lanthanides could substitute for Sr^{2+}: $LaNO_3$, $TbNO_3$, $EuNO_3$, $HoCl_3$, $YtCl_3$ and $TbCl_3$. Lanthanides were added in concentrations in the range between 5-200 mM with and without addition of $SrCl_2$. However, addition of lanthanides caused more protein precipitation and initiated the formation of needles and very thin sheets, similar to the ones formed in the presence of Ca^{2+}.

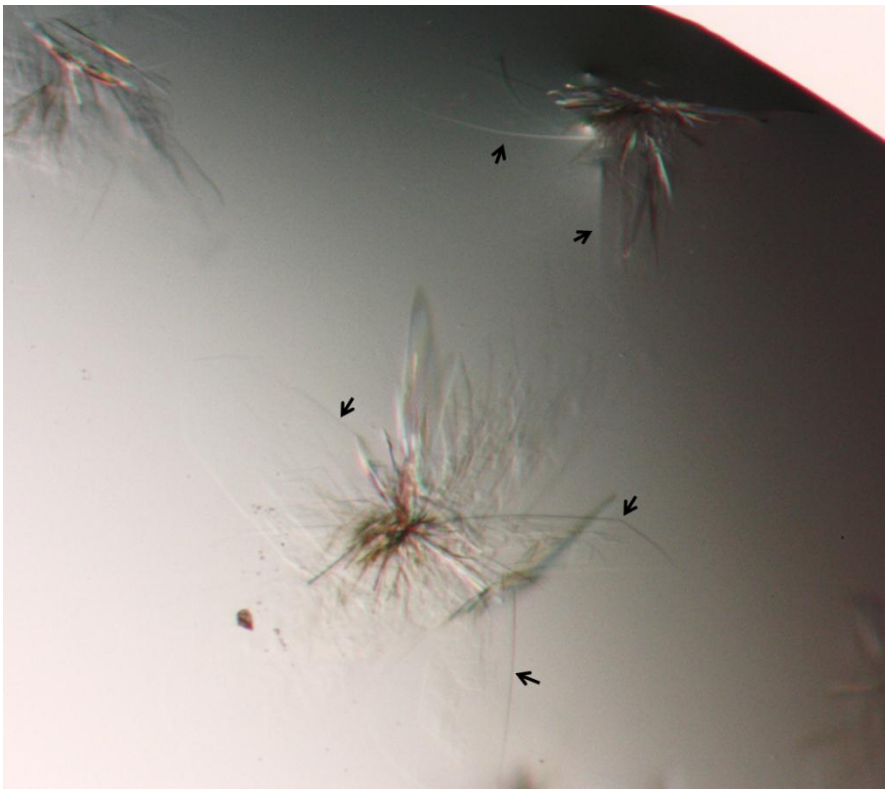

Figure 8. **RsaA$_{\Delta 0\text{-}222}$ crystalized using the hanging drop method.**
The drop was a mix of 4µl protein sample ((3 mg/mL) in 25 mM NaCl and 5 mM Tris) and 2 µL of precipitant (20% w/v PEG8000, 200 mM Calcium acetate and 0.1M MES pH 6)). The plate was incubated at 4°C. Sheets are indicated with arrows. Time needed to form these crystals was 2 weeks.

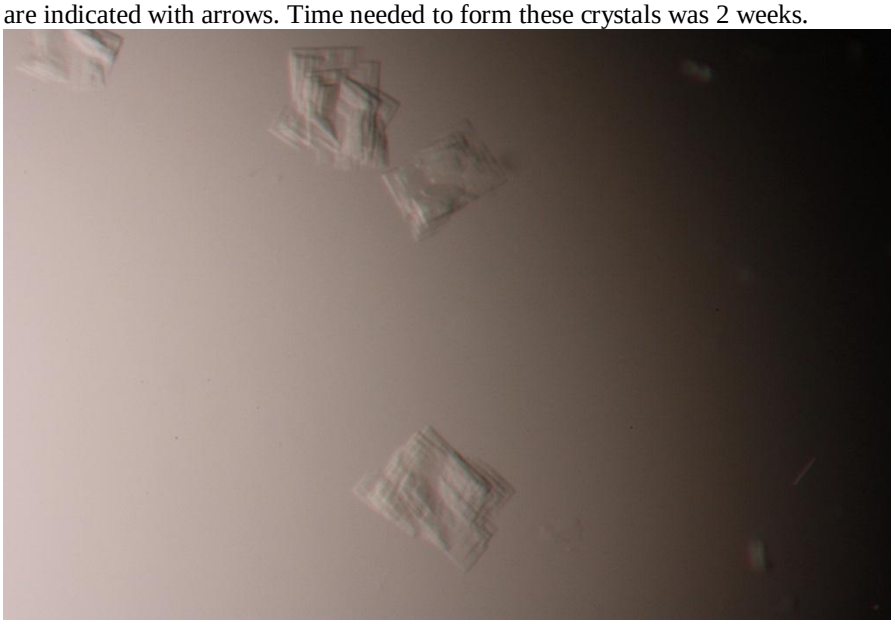

Figure 9. RsaA$_{\Delta 0\text{-}222}$ crystalized using the hanging drop method.
The drop was a mix of 4 µL of protein sample ((4 mg/mL) in 25 mM NaCl and 5 mM Tris) and 2 µL of precipitant (20% w/v PEG8000, 0.2M strontium chloride and 0.1M Tris pH7.5)). The plate was incubated at 4°C. Time needed to form these crystals was 5 weeks.

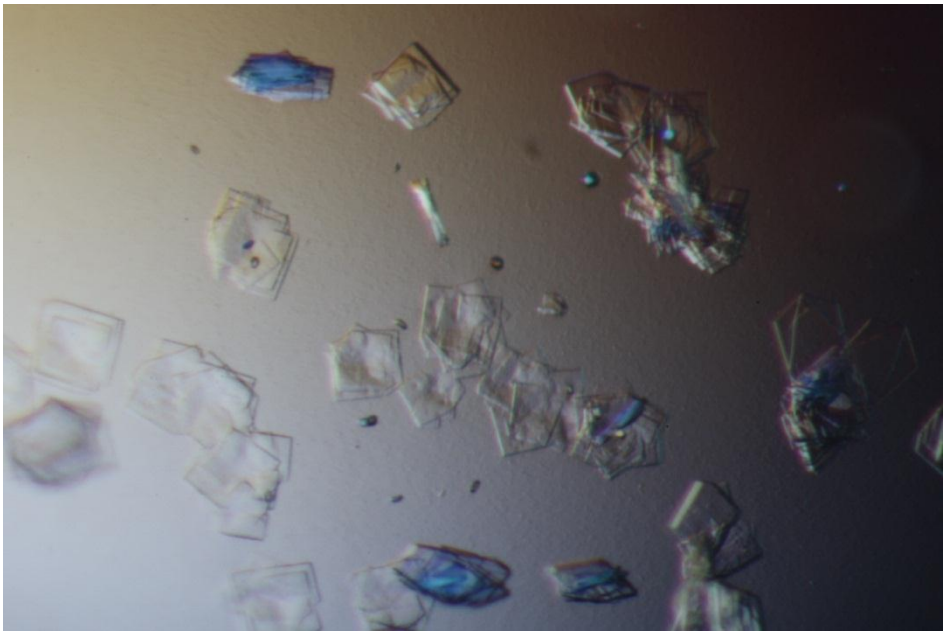

Figure 10. RsaA$_{\Delta 0\text{-}222}$ crystalized using the hanging drop method.
The drop was a mix of 4 µL of protein sample ((7 mg/mL) in 25 mM NaCl, 0.l% CHAPS and 5 mM Tris) and 2 µL of precipitant (20% w/v PEG8000, 0.2M strontium chloride and 0.1M Tris pH7.5)). The plate was incubated at 4°C. Crystals were a bit bigger and more clustered than the ones formed under the same conditions but at a lower sample concentration. Time required to form these crystals was 5 weeks.

3.3 S-layer protein crystals show only low resolution diffraction patterns

The crystals obtained with 200 mM Calcium acetate and Strontium chloride were used for x-ray diffraction experiments. In the first case, single crystal sheets were too thin to deliver a diffraction pattern. When a whole cluster of sheets and needles was placed in the beam, a few diffraction spots would appear, probably indicating the presence of salt (**Figure 11A**). The crystals obtained with $SrCl_2$ diffracted (**Figure 11B**), but the resolution was too low to derive further information such as space group and unit cell.

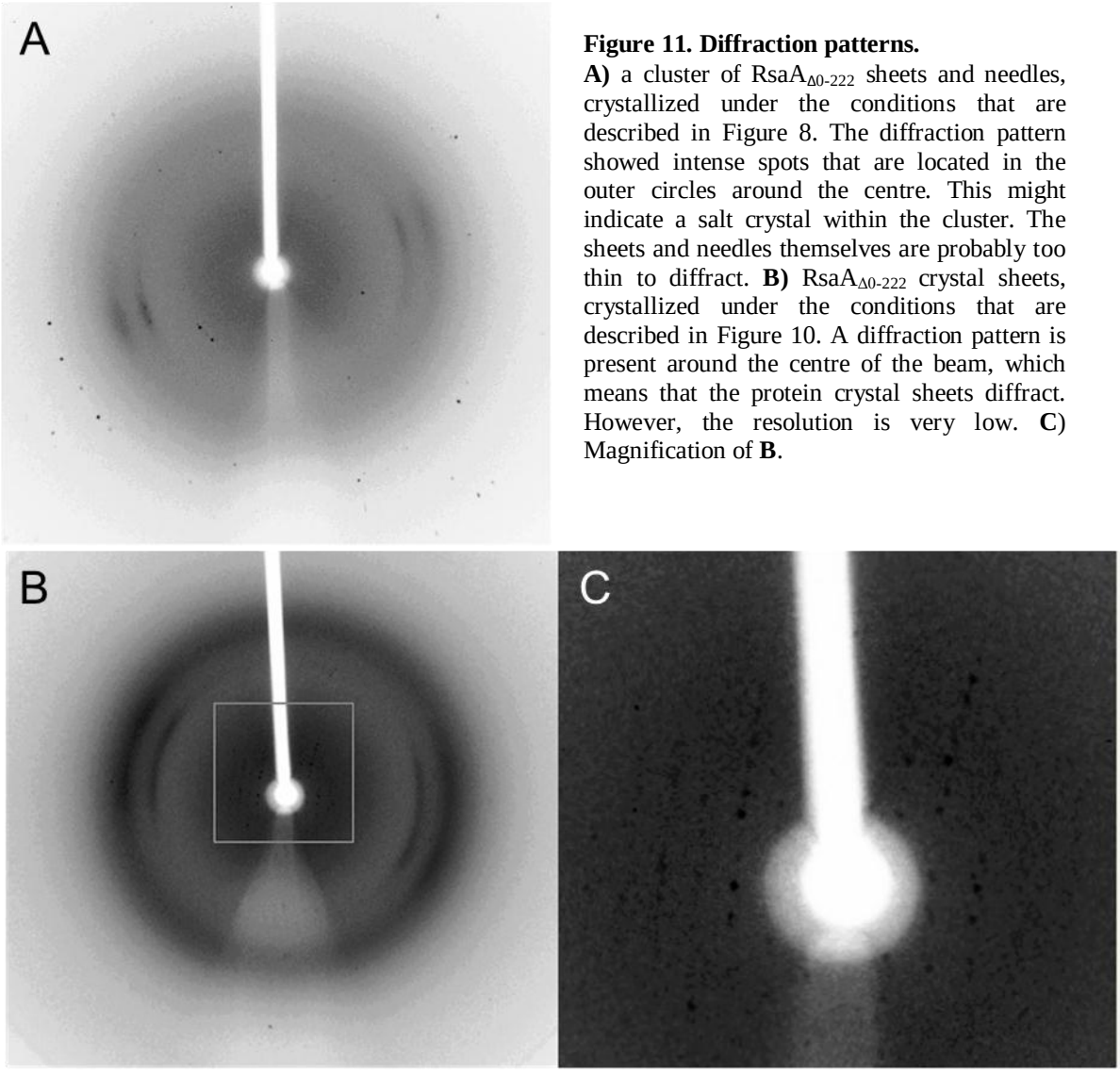

Figure 11. Diffraction patterns.
A) a cluster of $RsaA_{\Delta 0\text{-}222}$ sheets and needles, crystallized under the conditions that are described in Figure 8. The diffraction pattern showed intense spots that are located in the outer circles around the centre. This might indicate a salt crystal within the cluster. The sheets and needles themselves are probably too thin to diffract. **B)** $RsaA_{\Delta 0\text{-}222}$ crystal sheets, crystallized under the conditions that are described in Figure 10. A diffraction pattern is present around the centre of the beam, which means that the protein crystal sheets diffract. However, the resolution is very low. **C**) Magnification of **B**.

3.4 Characterization of nanobody-RsaA binding

To test which nanobodies bind accessible epitopes in the S-layer, S-layer positive cells were incubated with the nanobodies, which were then fluorescently labeled and investigated by phase contrast and fluorescence microscopy (examples are shown for Nb 5 and 10 in **Figure 12**). Nb 5, 7, 9 and 10 bound S-layer strongly and Nb 8 bound the S-layer with lower affinity. The other nanobodies (1, 2, 3, 4 and 6) did not interact with assembled S-layers. Those 5 nanobodies are potential candidates for binding regions, responsible for S-layer assembly.

Next, spot blots were done to test which nanobodies could bind isolated RsaA protein (**Figure 13**). All 10 nanobodies could bind individual RsaA proteins. Subsequently, western blots were done, to test whether the nanobodies could bind denatured full-length RsaA (thus linear epitopes). All nanobodies, except for Nb 4 emitted a signal in these western blots, indicating that Nb 4 binds a conformational epitope of RsaA (**Figure 13**). To limit the range where the binding site of each nanobody is localized, western blots were performed with different N-terminal protein truncates: $RsaA_{\Delta 0\text{-}690}$, $RsaA_{\Delta 0\text{-}784}$ and $RsaA_{\Delta 0\text{-}892}$. In addition, a mutant protein was used of which the N-terminus was fused to the extreme C-terminus: $RsaA_{\Delta 230\text{-}944}$. An important observation was that all nanobodies bind within the last 336 amino acids of RsaA (thus the C-terminus). Six nanobodies (3, 5, 7, 8, 9 and 10) bind between amino acid 784 and 892. Nb 1 and 4 bind between amino acid 690 and 784 and the remaining 2 bind between amino acid 784 and 892. None of the nanobodies bind the most C-terminal 82 amino acids. A visual representation of the nanobody characteristics is given in **Figure 13**.

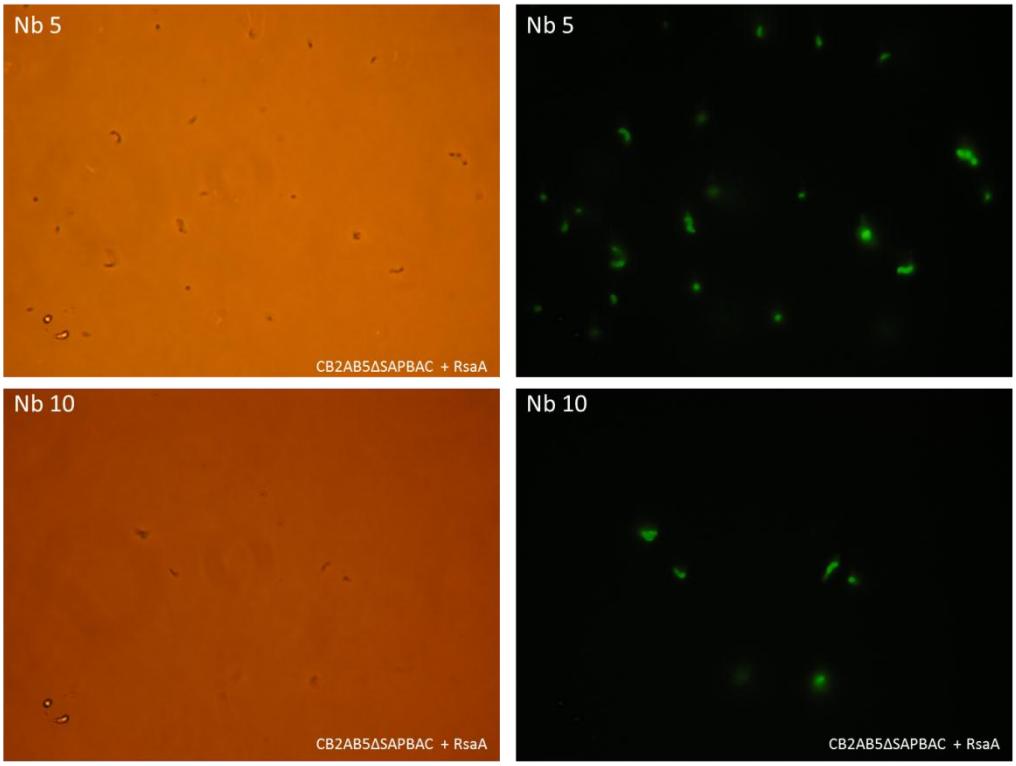

Figure 12. Nanobodies binding accessible epitopes in the S-layer.
Nb 5 and Nb 10 (i.e. 2 of 5 Nbs that bind fully formed S-layer) were visualized by epifluorescence with Nb - rabbit anti-His- goat anti-rabbit conjugated with Alexa Fluor® 488 (right panels). Phase contrast (left panels).

S-layer positive JS4026 (CB2AB5ΔSAPBAC complemented with p4B:*A19*. Controls were done with S-layer negative JS4026 (not shown).

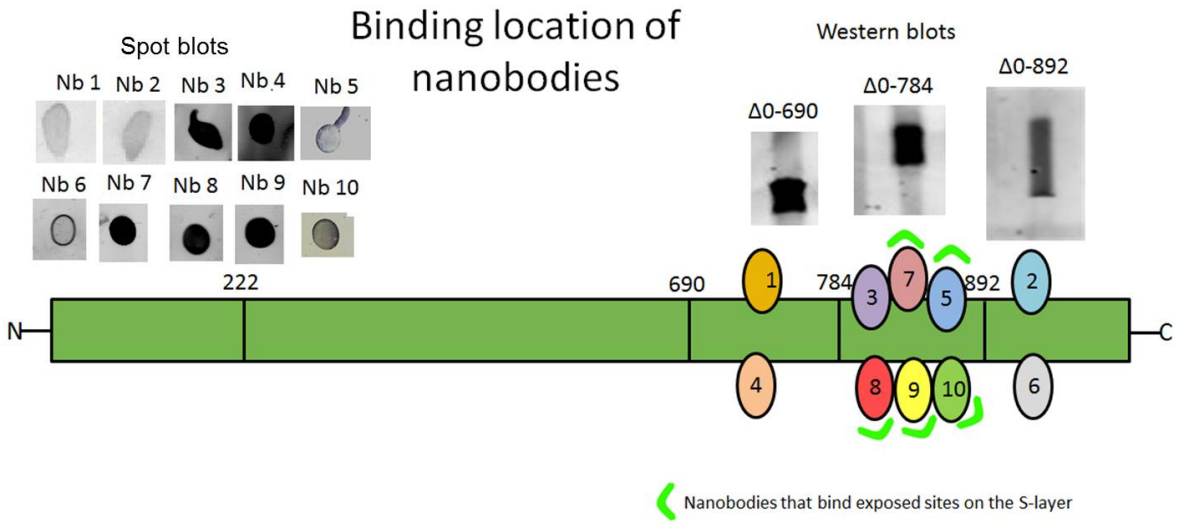

Figure 13. Linear representation of the regions that each nanobody binds in the amino acid sequence of RsaA.
The nanobodies that bind exposed sites on the formed S-layer are marked by the crescent shaped symbols. The 5 Nbs that bind exposed surfaces all bind in the region between AA784-AA892. Examples of western blots for nanobodies that bind the respective truncates are shown in the upper right. Spot blots for all 10 Nbs are shown in the upper left.

3.5 Isolation and assessment of nanobody-RsaA complexes

Nanobodies that bind a non-accessible epitope in the S-layer were chosen to focus on. Nb 3-RsaA$_{\Delta 0\text{-}222}$ complex could be isolated at low concentrations (~500 µg/mL) (**Figure 14**). However, the majority of nanobody was not properly bound and eluted later than the complex, whereas the majority of RsaA$_{\Delta 0\text{-}222}$ eluted earlier. The binding in the complex appeared to be even weaker when Nb 1 and Nb 6 were tested, for which I did not succeed in isolating complex at all. The Nb3- RsaA$_{\Delta 0\text{-}222}$ complex was concentrated to 2 mg/mL and assessed. Polydispersity values were higher than when no Nb was present.

Then, it was tested whether improvements in polydispersity were visible when Nbs were added to RsaA samples (**Table 4**). Polydispersity values were higher when Nb was added.

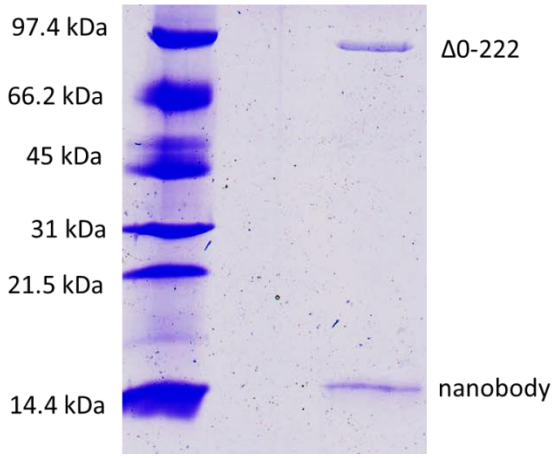

Figure 14. 13% Coomassie stained SDS-PAGE gel showing the purification of Nb3-RsaA complex.

Table 4. Precrystallization nanobody screen.

Nanobody	% polydispersity
1	53.5
3	27.3
4	26.7
6	21.5
8	60.2

* several nanobodies were added to a monodisperse $RsaA_{\Delta 0\text{-}222}$ sample (2 mg/mL;in 25 mM NaCl and 5 mM Tris pH7.5; polydispersity = 12.5%) and polydispersities were measured using DLS.

3.6 Prediction of aggregation inducing regions

Using TANGO software, it was predicted that an extremely hydrophobic region is present in the C-terminus of RsaA: T729-744. The program identified a very high propensity to aggregate by β-sheet formation in this region. Therefore, if this region would be disturbed, it might have an effect on the aggregation propensity as well as the folding properties of RsaA. A substitution mutation was made by site directed mutagenesis replacing valine at position 738 by aspartate. However, severe cloning problems have obstructed this approach as was described in section **2.2.3**.

3.7 Evaluation of RTX-impaired clones and libraries

Two clones with modified RTX regions (i.e. JS4026 with p4B:*Mtot1* and p4B:*ΔEcoRV*) were tested for protein shedding by colony western assays. None of the clones showed a signal, indicating that no S-layer is present on the bacterial surface. Secretion of S-layer was tested by low pH extraction of S-layer protein and checking for presence of protein on an SDS-

PAGE gel. Indeed, no protein was present, indicating that RTX regions are essential for secretion.

The libraries with insertion of *Bam*HI and pilin epitopes in the non-shedding strain JS4026 were tested several times in colony western assays. No mutants in which the protein was shed, were observed, meaning that the tested mutants were all capable to assemble RsaA into an S-layer.

4. S-layer protects against antimicrobial peptides

4.1 Protection against antimicrobial peptides mediated by the S-layer

To evaluate whether the S-layer of *C. crescentus* offered protection against antibiotics, an assay based on measuring optical densities of cell cultures after 24 hours, was designed. This showed that the S-layer positive strain JS4026 with p4B*RsaA600* was more resistant to cationic peptides LL37, 1018 and 1037 than the S-layer negative strain JS4026. To confirm this S-layer driven resistance, semi-high throughput assays, using 96-well plates were set up. Isogenic S-layer positive (NA1000) and S-layer negative strains (JS1013) were treated with increasing concentrations of peptide- and non-peptide antibiotics. This showed that the S-layer conferred variable levels of protection against all peptides, except against the negatively charged lipopeptide daptomycin (**Figure 16** and **Figure 17**). In contrast, no protection was seen when the strains were tested with non-peptide antibiotics (**Figure 18**). Protection percentages in these figures were calculated by subtracting survival values for JS1013 from the survival values for NA1000. As an example, a separate representation of the survival values for both strains treated with LL37 are given in **Figure 15**. The recorded MICs revealed that, in most cases, the S-layer was able to increase resistance to antimicrobial peptides by at least 2-fold (**Table 5**). The greatest level of protection was observed against the highly cationic peptide LP1.

A growth curve was also performed to compare treated and untreated NA1000 and JS1013 (**Figure 19**). At 2µg/mL LL-37, NA1000 grew to levels comparable to the untreated after 24 hours, whereas JS1013 was completely killed.

4.2 Killing assays show the protection level

In order to further assess the level of protection offered by the S-layer, killing assays were performed, which provide a more sensitive result than optical density readings or MIC measurements. Killing assays were performed by recording CFUs (colony forming units) at different time points after treatment with the peptides LL37 and LP1. This illustrated that the S-layer positive strain (NA1000) exhibited a ~10000-fold increase in survival when treated with 4 µg/mL LP1 and ~100-fold when exposed to 2 µg/mL LP1 compared to the S-layer

negative strain (JS1013) (**Figure 20A**). Likewise, the S-layer offered ~100-fold protection against 2 µg/mL LL37 (**Figure 20B**).

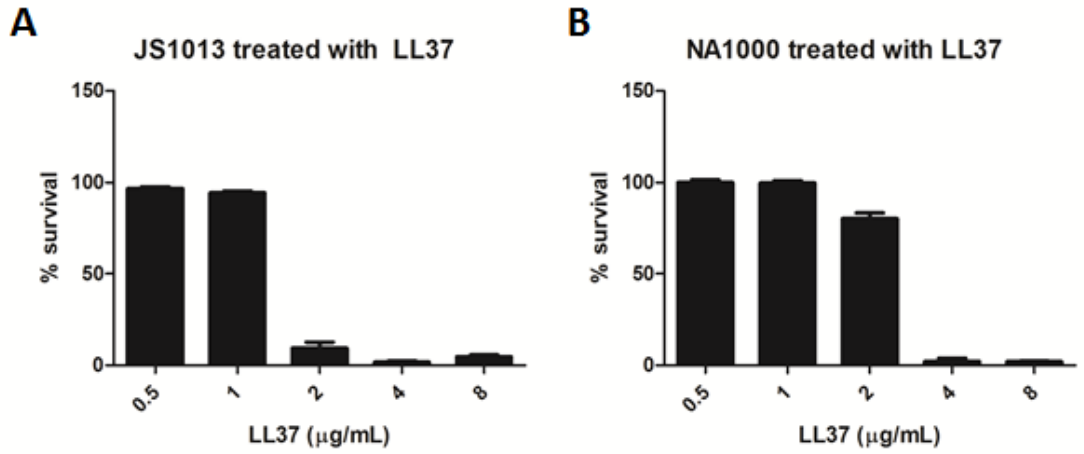

Figure 15. Survival curves for A) JS1013 and B) NA1000, when treated with LL37.
OD_{600} values were recorded after 24 hours and were converted into percentages by dividing the values obtained, by the average of their respective negative controls (i.e. no peptide treatment). These values represent survival percentages (Y-axis).

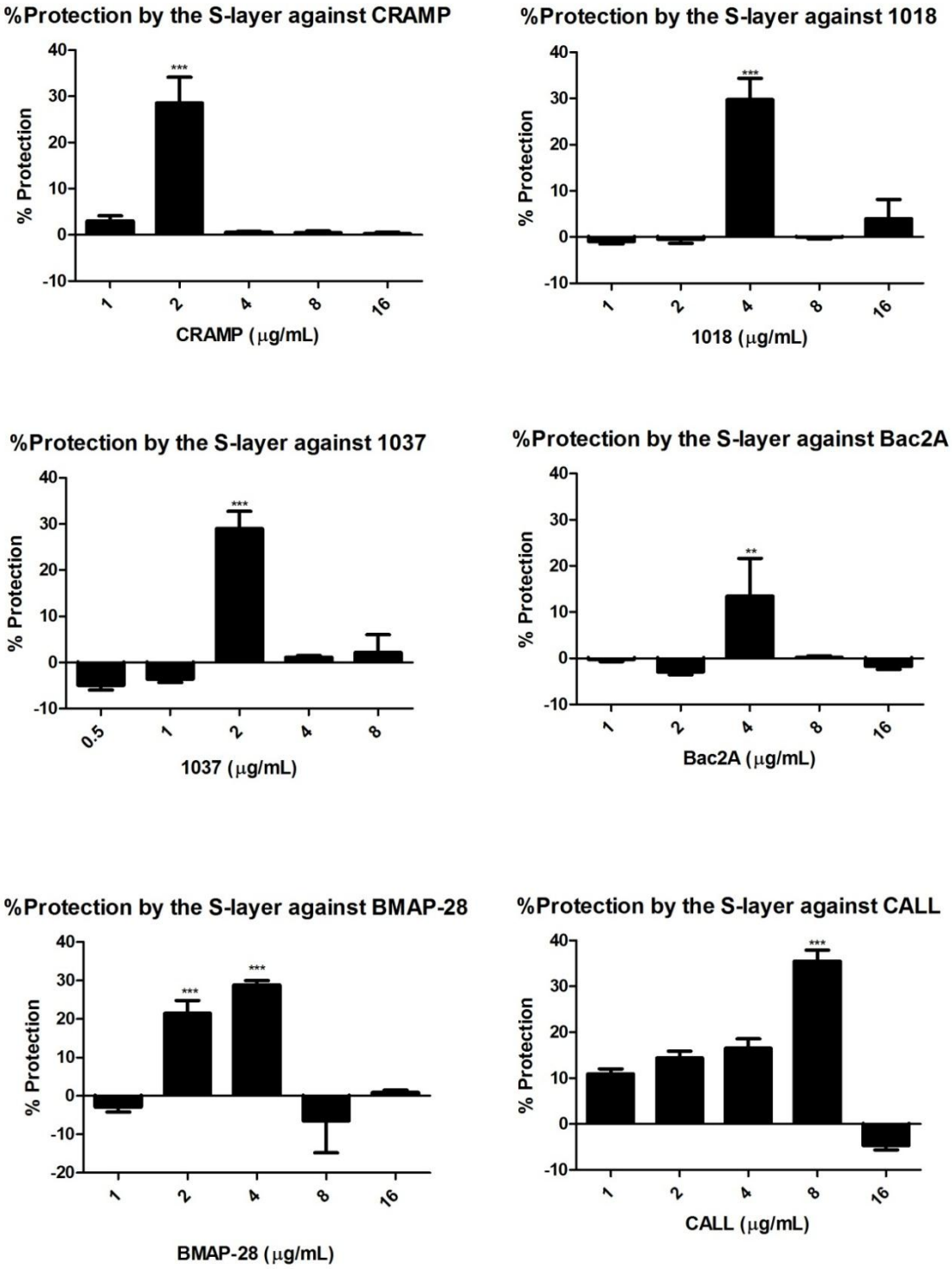

Figure 16. Protection graphs. The amount of protection offered by the S-layer when treated with different concentrations of antimicrobial peptides.
A two-way ANOVA was performed on all data to assess interaction between S-layer and concentration. t-tests were performed to assess significance levels at each concentration. Strains: NA1000 (S-layer positive) and JS1013 (S-layer negative). * indicates the significance level.

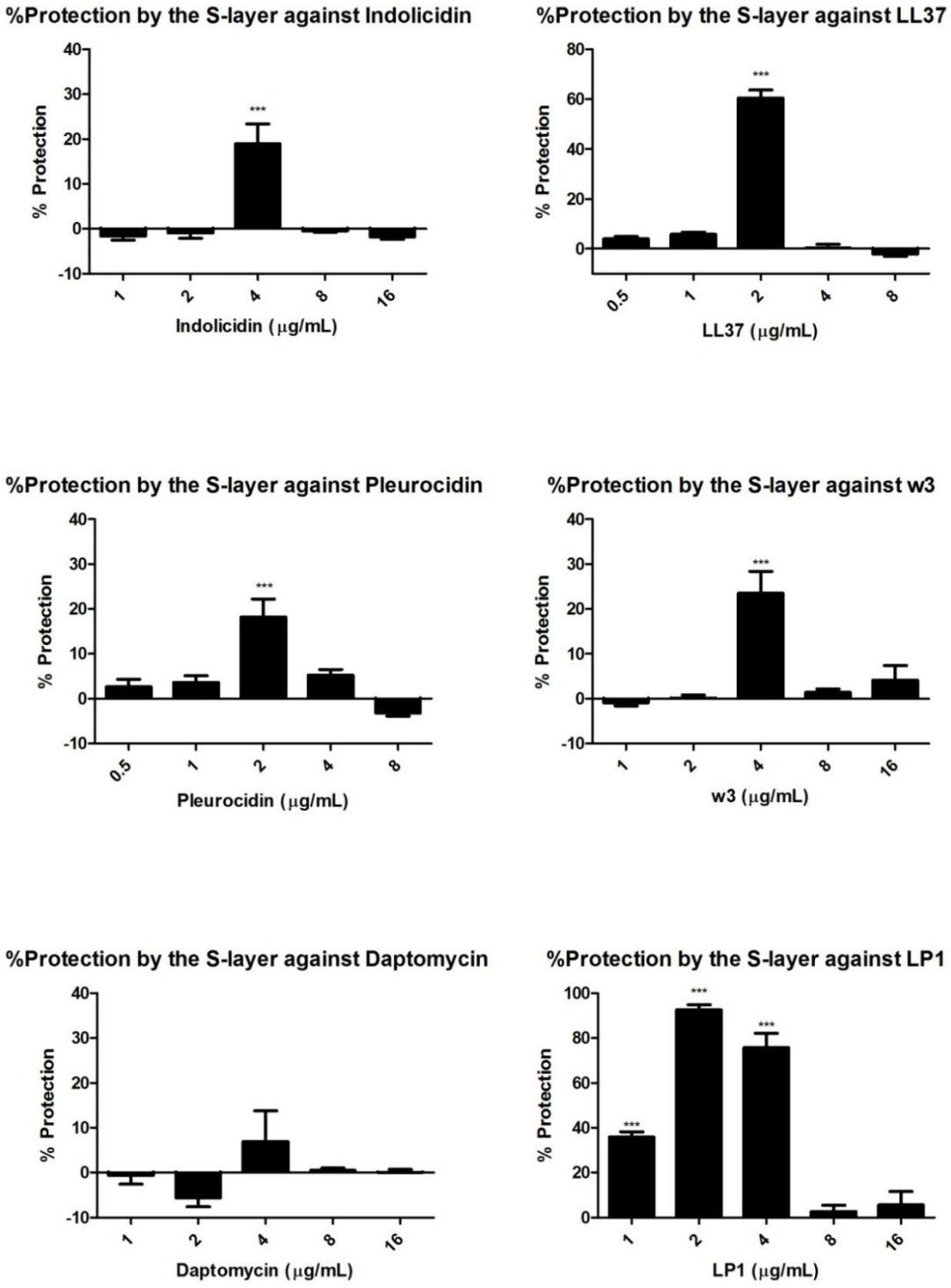

Figure 17. Protection curves.
The amount of protection offered by the S-layer when treated with different concentrations of antimicrobial peptides. A two-way ANOVA was performed on all data to assess interaction between S-layer and concentration. t-tests were performed to assess significance levels at each concentration. Strains: NA1000 (S-layer positive) and JS1013 (S-layer negative). * indicates the significance level.

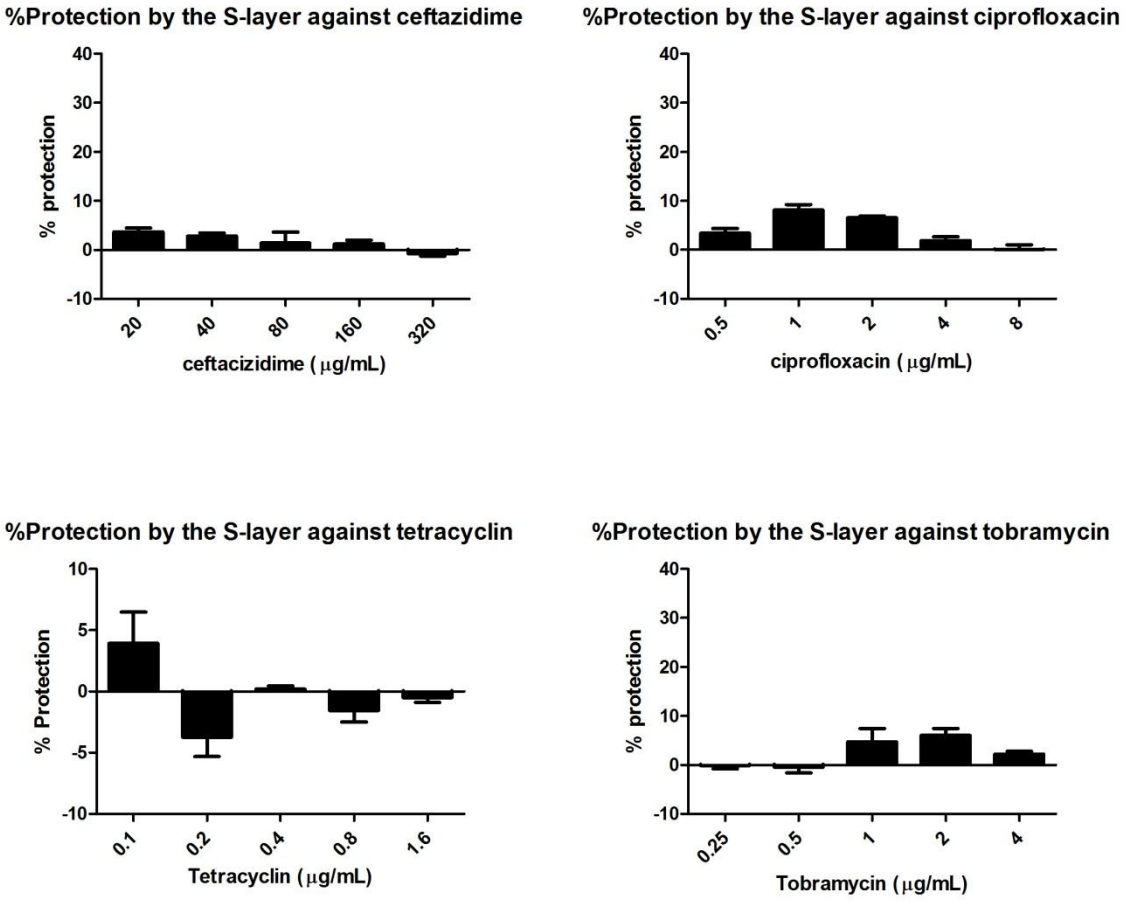

Figure 18. No protection was offered by the S-layer when treated with different concentrations of non-peptide antibiotics.

A two-way ANOVA was performed on all data to assess interaction between S-layer and concentration. t-tests were performed to assess significance levels at each concentration. Strains: NA1000 (S-layer positive) and JS1013 (S-layer negative). * indicates the significance level.

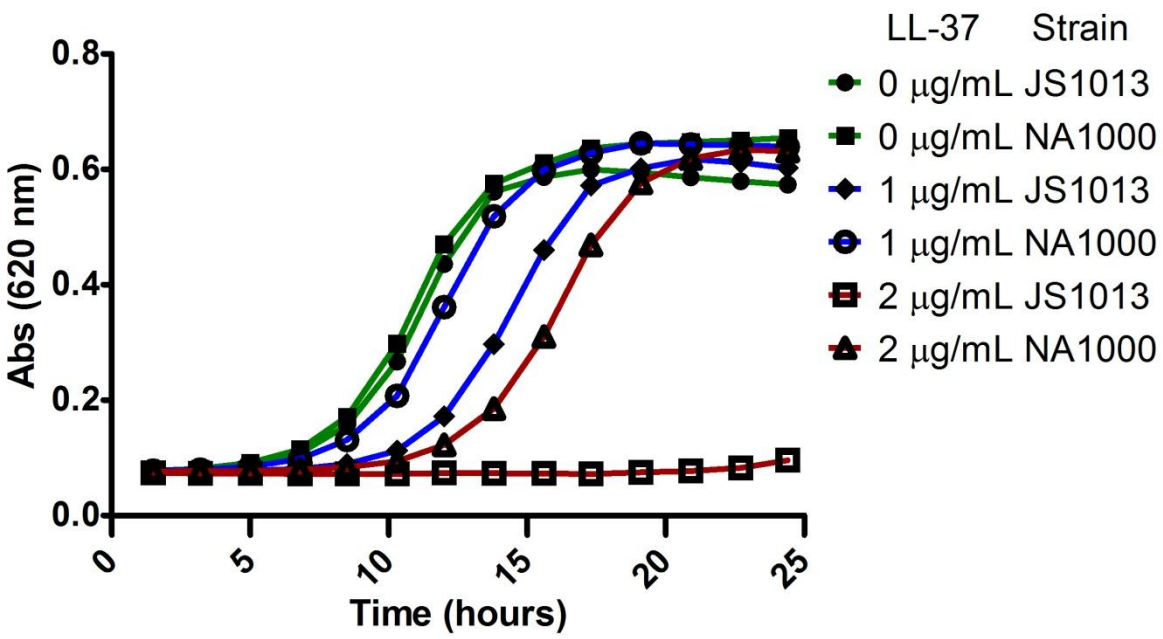

Figure 19. Growth curves for JS1013 and NA1000 subjected to different concentrations of LL37. Significant protection is observed at 1 and 2 μg/ml LL-37 as the S-layer positive strain NA1000 grows to levels equivalent to those of the untreated sample, while the S-layer negative strain is completely killed. NA1000 (S-layer positive) and JS1013 (S-layer negative).

Table 5. Antimicrobial peptides and their MIC values recorded after 24 hours for JS1013 and NA1000

Peptide	Amino acid sequence	Molecular weight (g/mol)	Charge	MIC (µg/mL) S-layer negative JS1013	MIC (µg/mL) S-layer positive NA1000
LP-1	RKRKRKRKR(K-myristoyl)	1512.6	+9	2	8
CALL	KWKLFKKIFKRIVQRIKDFLR	2791.5	+8	8	16
BMAP-28	GGLRSLGRKILRAWKKYGPIIVPIIRIG	3130.9	+7	4	8
CRAMP	ISRLAGLLRKGGEKIGEKLKKIGQKIKNFFQKLVPQPE	4291.2	+7	2	4
LL-37	LLGDFFRKSKEKIGKEFKRIVQRIKDFLRNLVPRTES	4391.3	+6	2	4
1037	KRFRIRVRV	1229.5	+5	2	4
Bac2A	RLARIVVIRVAR	1421.8	+4	4	8
1018	VRLIVAVRIWRR	1536.9	+4	4	8
W3	VRWIVAVRIWRR	1610.0	+4	4	8
Pleurocidin	GWGSFFKKAAHVGKHVGKAALTHYL	2711.2	+4	2	4
Indolicidin	ILPWKWPWWPWRR	1907.3	+3	4	8
Daptomycin	n-decanoyl-WN^{D}DTGODA^{D}DGS^{D}TEK[1]	1619.7	-3	8	8

[1] N^{D} signifies the D isomer of asparagine for example; O = ornithine; K= kynurenine

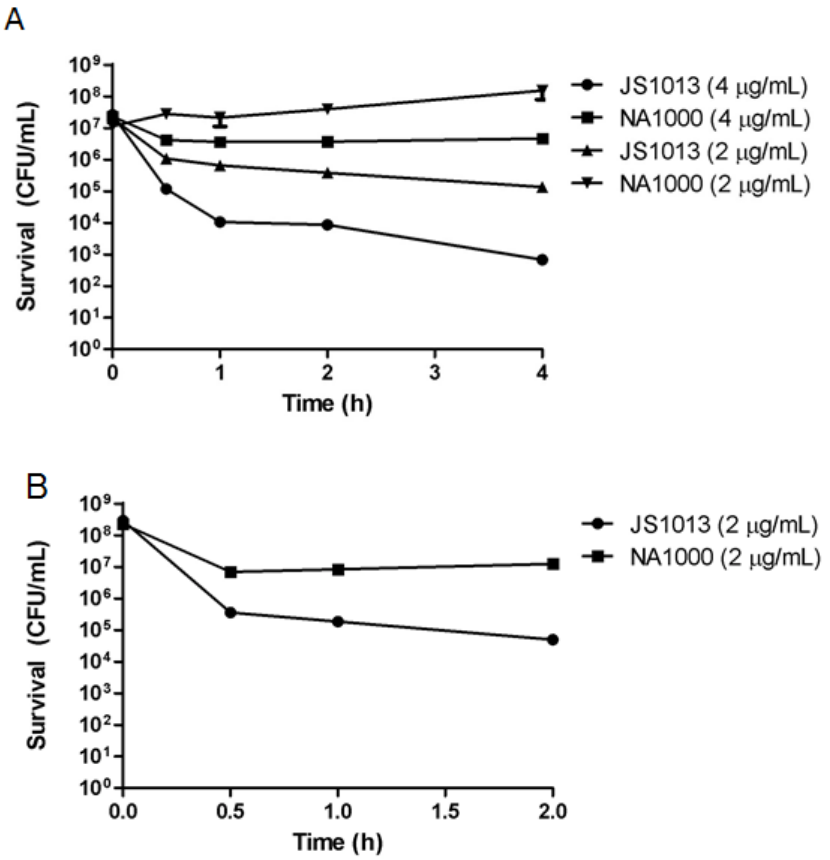

Figure 20. Killing curves for JS1013 (S-layer negative) and NA1000 (S-layer positive).
A) After 4 hours 10000-fold and 100-fold differences in survival are observed when treated with 4 µg/mL LP1 and 2 µg/mL LP1 respectively. **B)** After 2 hours a 100-fold difference in survival is observed when treated with 2 µg/mL LL37.

4.3 The S-layer offers protection to biofilm cells

To investigate whether S-layers protect *C. crescentus* when grown in biofilms, the biofilm-forming strains CB15 (S-layer positive) and CB15ΔRsaA (S-layer negative) were used. Both were treated with increasing concentrations of LP1 and LL37. Biofilms formed by CB15 exhibited increased resistance to LL37 and LP1 when compared to CB15ΔRsaA (**Figure 21)**. A more detailed explanation of this experiment can be found in the legend of **Figure 21**.

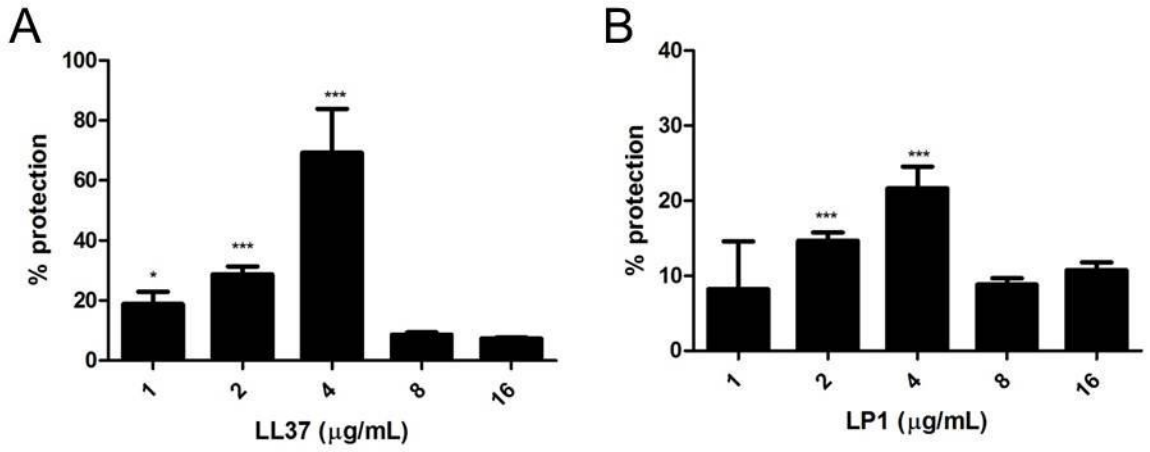

Figure 21. The S-layer provides protection in biofilms against increasing concentrations of antimicrobial peptide A) LP1, and B) LL37.
A two-way ANOVA was performed on all data to assess interaction between S-layer and concentration. t-tests were performed to assess significance levels at each concentration. Optical densities (OD_{600}) of biofilm, after crystal violet staining, were measured for peptide-treated samples of both S-layer positive (CB15) and S-layer negative (CB15ΔRsaA) strains and the resulting OD_{600} values were converted into percentages by dividing the values obtained, by the average of their respective negative controls (i.e. no peptide treatment). The % protection level provided by the S-layer was calculated by subtracting the % values for the S-layer negative strain from the values of the S-layer positive strain at each peptide concentration.

4.4 Supplementation with exogenous RsaA confers protection to an S-layer negative strain

In order to determine whether the S-layer protein itself was sufficient to explain the protection observed, isolated RsaA was added in increasing concentrations to JS1013 (S-layer negative) treated with 2 µg/mL LL-37. 100% survival was observed when as little as 62.5 µg/mL RsaA protein was supplemented to the medium, suggesting that the S-layer protein is responsible for the protection observed (**Figure 22**).

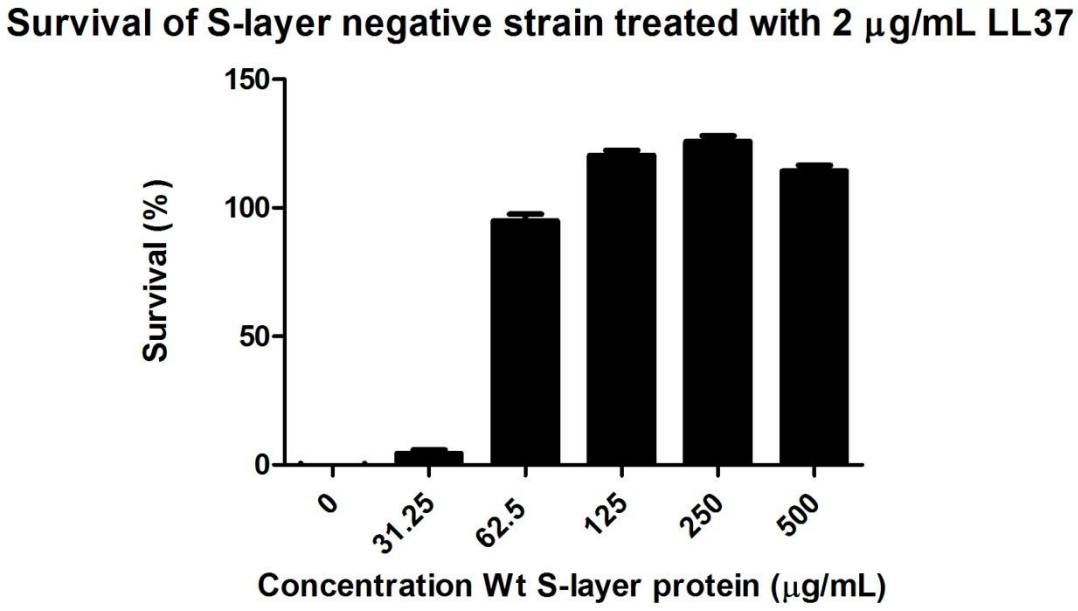

Figure 22. Exogenous addition of full-length S-layer protein to JS1013 (S-layer negative) restores protection against antimicrobial peptides.

4.5 S-layer prevents cationic peptides from interaction with outer membrane.

To obtain a visual assessment of the interaction between the S-layer and antimicrobial peptides, strains NA1000 and JS1013 were treated with increasing concentrations of B-LL37 for 30 min. Both S-layer and B-LL37 could be visualized by fluorescence as red and green respectively (**Figure 23**). The S-layer negative cells showed green fluorescent labeling at every concentration of B-LL-37 tested, but the signal was more intense at higher concentrations. Furthermore, cell lysis occurred with increasing concentrations of B-LL37. At 8 µg/ml, few intact cells were left and the presence of cell debris was noticed through phase contrast microscopy. For NA1000, green fluorescent labeling was only observed when using high levels of LL-37 (4-8 µg/ml). The lack of green labeling at lower concentrations indicates that the peptide at those levels could not interact with the outer membrane, most likely because of interaction with the S-layer. The interaction was probably not strong enough to prevent washout during the washing steps.

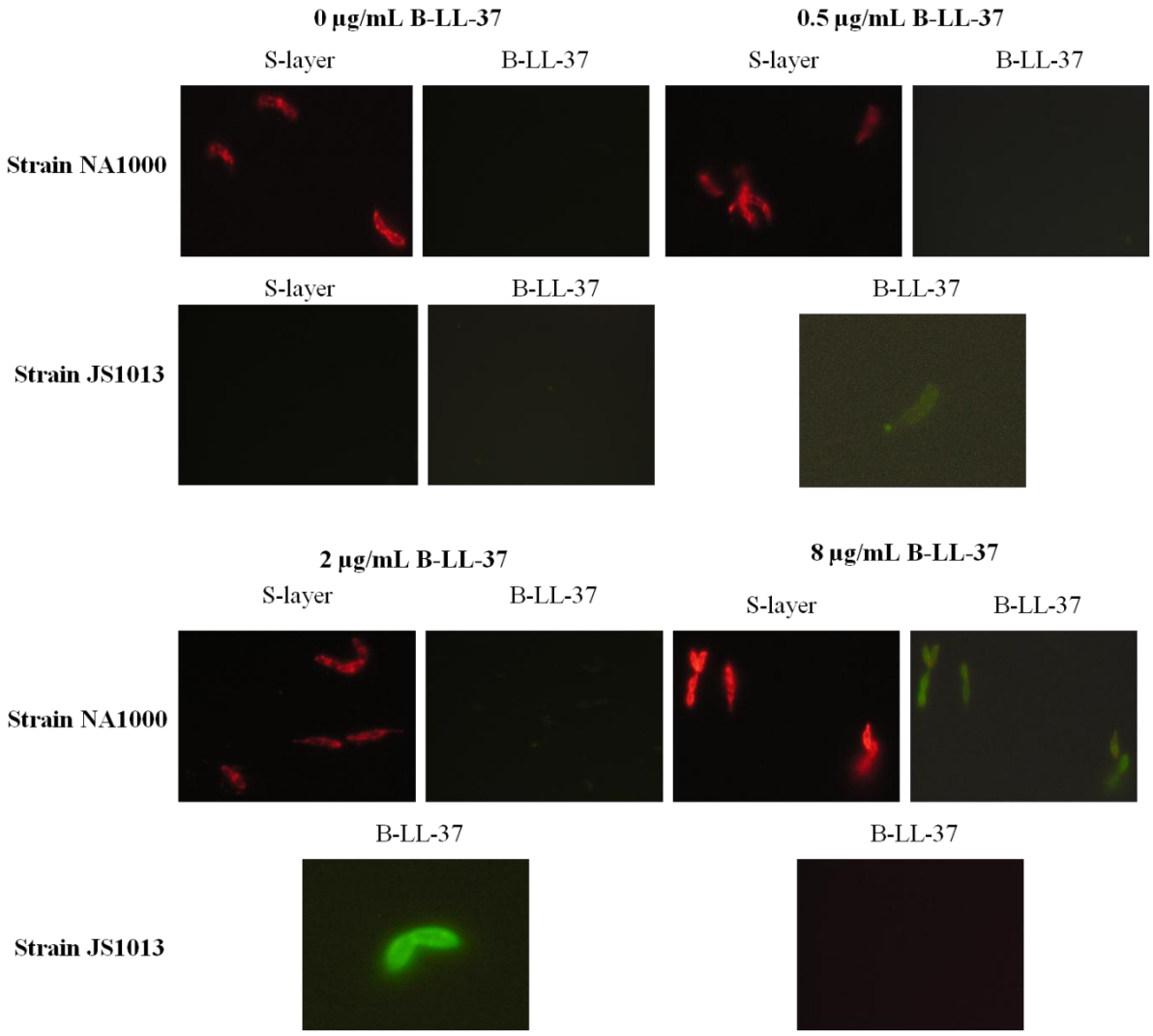

Figure 23.Visualization of susceptibility to cationic peptides.
Exogenously added biotinylated peptide LL-37 is unable to enter the outer membrane of S-layer positive cells (NA1000) at 2 µg/ml but does at 8 µg/ml. B-LL37 is inserted in the membrane of S-layer negative cells (JS1013) already at concentrations of 0.5 µg/ml. At higher concentrations, more cells were lysed. The S-layer was labeled with a polyclonal rabbit anti-RsaA antibody and a secondary goat anti-rabbitAlexaFluor® 568 and the exogenously added peptide B-LL-37 was labeled with streptavidin Alexa Fluor® 488.

5. Discussion and conclusion

The goal of this thesis was to develop methods to improve RsaA quality to a level required for crystallization. These crystals could then be tested in x-ray diffraction experiments to obtain an atomic-resolution structure of the S-layer protein. Working with RsaA provided initially a couple of advantages. Because RsaA is highly expressed and secreted into the extracellular environment, it was readily available for use. Thus, I could circumvent the first obstacles that scientists usually encounter when trying to crystallize a protein; i.e. constitute a stable expression system for the protein, that enables scaling up to produce quantities that are sufficient for crystallization (miligrams). Secondly, a reliable extraction method needs to be available that is not associated with high protein losses or compromises protein quality. In case of RsaA, the protein is already brought to the surface of the cell, thus no harsh extraction procedures, that would also introduce significant amounts of other protein impurities, are required. However, these advantages are compensated by the high propensity of RsaA to aggregate, which is an inherent characteristic shared by all different S-layers studied. For more than 20 years, this has been an important obstruction that has prevented the acquirement of high-resolution structures for S-layers. The issue can be subdivided into two subproblems: 1) high tendency to aggregate when concentrated to levels higher than present in nature, 2) the natural crystalline sheet formation as the acquirement of a third dimension is necessary to obtain a crystal that is thick enough for x-ray diffraction. The big challenge lies herein and the path that I followed throughout is characterized by a selection of methods by trial and error. The means had to be developed to prevent aggregation (monodipersity criterium) and increase concentration without deterioration of protein quality (concentration criterium). Important to note is that all methods used in this thesis can only work when a limited amount of domains are responsible for protein aggregation. If the aggregation propensity is an intrinsic property of the complete protein sequence, none of these methods would be able to circumvent aggregation completely.

A first question that rose when I started this project, was how protein should be collected. I chose to use an S-layer shedding strain, in which RsaA would not be able to attach to the outer membrane and could be readily collected from the supernatant. A low pH extraction method would have been an alternative method to extract S-layer protein from the cell surface of a non-shedding strain. However, this method introduces several other protein

impurities and a higher chance of compromising protein integrity exists. A pivotal discovery was that agitation of RsaA in solution should be minimized. Agitation increases interaction between RsaA proteins and hence results in augmented aggregate formation. Thus, S-layer shedding *C. crescentus* cultures had to be shaked at a very low rate. Similarly, protein was concentrated using aquacide II, which gently concentrates protein, nearly without losses. Previously centrifugal filters were used, favoring protein aggregation. An additional way to concentrate protein and enable stable long term storage, was lyophilization of supernatant from S-layer shedding cultures. Based upon these observations, a straightforward protocol of methods was designed to consistently prepare protein samples.

Full-length RsaA was highly unstable compared to the tested N-terminally truncated proteins. Full-length RsaA would form high-molecular weight aggregates at every concentration attempt. Using DLS as an assessment tool, $RsaA_{\Delta 0\text{-}222}$ was proven to be the most stable RsaA truncate. Its initial upper concentration limit was 4 mg/mL and estimations of molecular weight by DLS software, indicated that $RsaA_{\Delta 0\text{-}222}$ was soluble as monomers. The concentration limit was driven upward to 9 mg/mL when solubilized with the neutral zwitterionic detergent CHAPS. However, 7 mg/mL was the highest concentration at which protein was still monomeric. At 9 mg/mL a mixture of monomers and dimers was present, based upon the higher polydispersity values measured by DLS. Furthermore, the increased solubility of $RsaA_{\Delta 0\text{-}222}$ compared to the full-length protein implies that a region in the N-terminus of RsaA is present that, by itself or by interaction with the C-terminus, induces aggregation. Important for the stable conformation of $RsaA_{\Delta 0\text{-}222}$ is also the presence of amino acids 222-551. This was demonstrated by the increase in aggregation of the smaller N-terminal truncates $RsaA_{\Delta 0\text{-}551}$ and $RsaA_{\Delta 0\text{-}690}$.

Crystal screens showed that divalent cations are necessary for crystallization (i.e. Ca^{2+} or Sr^{2+}). RsaA contains six RTX domains, which are known to bind calcium. Binding with divalent cations might be necessary for the overall structure of the protein. The best crystals were obtained when $RsaA_{\Delta 0\text{-}222}$ (0.1% CHAPS, 25 mM NaCl, 5 mM Tris) was used in combination with 200 mM, $SrCl_2$ 20% w/v PEG8000 and 100 mM Tris pH 7.5. These crystals formed after 5-6 weeks and were tested using x-ray diffraction. A protein diffraction

pattern was observed, but the resolution was too low to extract information such as the space group and the unit cell.

Ten RsaA-binding nanobodies were characterized in this thesis. Five nanobodies that bound accessible regions on the S-layer were found, whereas five other nanobodies were found to bind non-exposed regions that are candidates for involvement of S-layer assembly. Interestingly, the binding sites for the Nbs that bind accessible S-layer regions are all located between residue 784 and 892. This indicates that this region is exposed in the S-layer. In addition, none of the nanobodies bind within the first 690 amino acids of RsaA, which could mean that this region is not accessible. Nanobody binding was found to be not strong enough to form stable RsaA-Nb complexes and were thereby not useful in the crystallization studies.

Aggregation prediction software (TANGO) identified one region in the C-terminus of RsaA with a very high aggregation propensity in $RsaA_{\Delta 0\text{-}222}$ between T729-T744. Hence, this region might be responsible for instability of the truncate.

A mutant in which 2 RTX domains in RsaA were deleted and a mutant in which the last amino acid of the last RTX domain was deleted, could not secrete protein at all. This indicates that these RTX domains might be important for the overall protein folding and necessary for protein secretion.

We can conclude that the property of RsaA to assemble into sheets presents itself as well in crystallization trials and this proves to be very hard to overcome. This work shows that RsaA truncated proteins can be crystallized and, given the right conditions, can reach a limited thickness. In order to obtain high quality diffraction data, conditions should be found that lead to thicker crystals.

Currently, we cannot predict the quality of the crystals and their diffraction characteristics. In addition, RsaA mutants might not be folded into a conformation that represents their state within S-layer proteins. Overall, we can say that S-layers are still one of the many examples in which production of high-quality crystals is a bottleneck in structure determination [48]

The second objective of my thesis was to test whether the S-layer conferred protection against antimicrobials. MIC assays, and growth curves showed that the S-layer of *C. crescentus* protects against antimicrobial peptides but not against non-peptide antibiotics. This is probably due to the high amount of positive charges that are present in antimicrobial peptides. Indeed, no protection by the S-layer was observed against the negatively charged lipopeptide daptomycin and high levels of protection were observed when cells were treated with the highly cationic peptide LP1. The protective effect was also shown when cells were grown in biofilms. The increased resistance comparing S-layer positive with S-layer negative strains was at least 2-fold. This is particularly interesting for bacterial survival in non-human manipulated settings in which a 2-fold increase in antimicrobial peptide levels is very unlikely to occur as these peptides are produced by virtually all organisms in low concentrations in unchanging, diluted niches [37,38]. Killing curves allowed a more accurate measurement of cell killing than MICs [49] and emphasized the protection offered by the S-layer against antimicrobial peptides. Also, as antimicrobial peptides rapidly kill bacteria, the shorter time points used in killing assays (2-4 h) covered the time interval of direct cell killing better.

The mechanism of protection could be due to interactions of the acidic S-layer with the positively charged peptides. Interestingly, most S-layers have low isoelectric points (thus a net negative charge), except for the S-layers of *Lactobacilli* (**Table 6**). Other studies also show that some surface structures function to protect prokaryotes against antimicrobials. For example, *Klebsiella pneumonia* is covered by a polysaccharide capsule that confers protection against antimicrobial peptides [50]. A capsule negative mutant was more sensitive to human neutrophil defensin 1, β-defensin 1, lactoferrin, protamine sulfate, and polymyxin B than the wild type bacterium. This is also comparable to a study done with the human fungal pathogen *Candida albicans*[51]. This pathogen possesses a sensor protein Msb2 in the plasma membrane that also offers protection against antimicrobial peptides (e.g. LL37 and histatin-5). When added exogenously to fungal or bacterial pathogens, the protective effect could be observed as well. Similarly, the authors propose that protection occurred because of interaction between charges. They suggest that anionic groups of Msb2 (carboxylate side chain of aspartates and glutamates) interact with the antimicrobial peptides. This theory can

also be applied on the S-layer as it contains a lot of carboxylate side chains (mainly from aspartates but also some glutamates).

This leads to my hypothesis that microorganisms could use surface structures to shield the negatively charged outer cell membrane by a negatively charged coating (e.g. S-layer, sensor protein, polysaccharide capsule).

Table 6: Isoelectric point of S-layer proteins of different bacteria

Bacterium	**S-layer protein**	**pI**
Caulobacter crescentus	RsaA	3.46[19]
Campylobacter fetus	Type A Type B	4.2 [52] 4.4[52]
Corynebacterium glutamicum	PS2	4.11-4.27 [53]
Deinococcus radiodurans	Hpi SlpA	4.8[53] 4.9[53]
Lysinibacillus sphaericus	Various S-layer proteins	4.7-5.2 [53]
Aeromonas salmonicida	VapA	5.1[53]
Geobacillus stearothemophilus	SbsB	5.7[53]
Bacillus anthracis	Sap EA1	6 [53] 5.5[53]
Lactobacilli	mature S-layer proteins	9.4-10.4[53]

Overall, a new role was identified for the S-layer of *C. crescentus* that might be shared by other S-layer proteins, i.e. forming a protective barrier against antimicrobial peptides. These results challenge the previously assumed hypothesis that S-layers allow free passage of small

molecules. In environmental settings, this will provide S-layer positive bacteria with a survival advantage over S-layer negative cells. We suggest that S-layers have had a role as a resistance mechanism that allows bacterial survival when antimicrobial peptides are present in the environment, justifying its conservation throughout evolution. Thus, the S-layers in pathogenic bacteria such as *B. anthracis* and *C. fetus* may also serve as resistance barriers against antimicrobial peptides both in environmental and clinical settings.

Bibliography

1 Sleytr, U. B., Egelseer, E. M., Ilk, N., Pum, D. & Schuster, B. S-Layers as a basic building block in a molecular construction kit. *The FEBS journal* **274**, 323-334, doi:10.1111/j.1742-4658.2006.05606.x (2007).

2 Amat, F. *et al.* Analysis of the intact surface layer of *Caulobacter crescentus* by cryo-electron tomography. *Journal of bacteriology* **192**, 5855-5865, doi:10.1128/JB.00747-10 (2010).

3 Houwink, A. L. A macromolecular mono-layer in the cell wall of *Spirillum* spec. *Biochimica et biophysica acta* **10**, 360-366 (1953).

4 Houwink, A. L. Flagella, gas vacuoles and cell-wall structure in *Halobacterium halobium*; an electron microscope study. *Journal of general microbiology* **15**, 146-150 (1956).

5 Zafiu, C., Trettenhahn, G., Pum, D., Sleytr, U. B. & Kautek, W. Structural control of surface layer proteins at electrified interfaces investigated by in situ Fourier transform infrared spectroscopy. *Physical chemistry chemical physics : PCCP* **13**, 13232-13237, doi:10.1039/c0cp02127j (2011).

6 Nomellini, J. F., Duncan, G., Dorocicz, I. R. & Smit, J. S-layer-mediated display of the immunoglobulin G-binding domain of streptococcal protein G on the surface of *Caulobacter crescentus*: development of an immunoactive reagent. *Applied and environmental microbiology* **73**, 3245-3253, doi:10.1128/AEM.02900-06 (2007).

7 Nomellini, J. F. *et al.* Development of an HIV-1 specific microbicide using *Caulobacter crescentus* S-layer mediated display of CD4 and MIP1alpha. *PloS one* **5**, e10366, doi:10.1371/journal.pone.0010366 (2010).

8 Duval, M. *et al.* Enhanced neutralization of HIV by antibodies displayed on the S-layer of *Caulobacter crescentus*. *Antimicrobial agents and chemotherapy* **55**, 5547-5552, doi:10.1128/AAC.00509-11 (2011).

9 Umelo-Njaka, E. *et al.* Expression and testing of *Pseudomonas aeruginosa* vaccine candidate proteins prepared with the *Caulobacter crescentus* S-layer protein expression system. *Vaccine* **19**, 1406-1415 (2001).

10 Bhatnagar, P. K., Awasthi, A., Nomellini, J. F., Smit, J. & Suresh, M. R. Anti-tumor effects of the bacterium *Caulobacter crescentus* in murine tumor models. *Cancer biology & therapy* **5**, 485-491 (2006).

11 Bingle, W. H., Nomellini, J. F. & Smit, J. Linker mutagenesis of the *Caulobacter crescentus* S-layer protein: toward a definition of an N-terminal anchoring region and a C-terminal secretion signal and the potential for heterologous protein secretion. *Journal of bacteriology* **179**, 601-611 (1997).

12 Sara, M., Pum, D. & Sleytr, U. B. Permeability and charge-dependent adsorption properties of the S-layer lattice from *Bacillus coagulans* E38-66. *Journal of bacteriology* **174**, 3487-3493 (1992).

13 Lau, J. H., Nomellini, J. F. & Smit, J. Analysis of high-level S-layer protein secretion in *Caulobacter crescentus*. *Canadian journal of microbiology* **56**, 501-514, doi:10.1139/w10-036 (2010).

14 Delepelaire, P. & Wandersman, C. Protein secretion in gram-negative bacteria. The extracellular metalloprotease B from *Erwinia chrysanthemi* contains a C-terminal secretion signal analogous to that of *Escherichia coli* alpha-hemolysin. *The Journal of biological chemistry* **265**, 17118-17125 (1990).

15 Toporowski, M. C., Nomellini, J. F., Awram, P. & Smit, J. Two outer membrane proteins are required for maximal type I secretion of the *Caulobacter crescentus* S-layer protein. *Journal of bacteriology* **186**, 8000-8009, doi:10.1128/JB.186.23.8000-8009.2004 (2004).

16 Nomellini, J. F., Kupcu, S., Sleytr, U. B. & Smit, J. Factors controlling in vitro recrystallization of the *Caulobacter crescentus* paracrystalline S-layer. *Journal of bacteriology* **179**, 6349-6354 (1997).

17 Smit, J. Heads up S-layer display: the power of many. *Structure* **16**, 1151-1153, doi:10.1016/j.str.2008.07.003 (2008).

18 Ford, M. J., Nomellini, J. F. & Smit, J. S-layer anchoring and localization of an S-layer-associated protease in *Caulobacter crescentus*. *Journal of bacteriology* **189**, 2226-2237, doi:10.1128/JB.01690-06 (2007).

19 Gilchrist, A., Fisher, J. A. & Smit, J. Nucleotide sequence analysis of the gene encoding the *Caulobacter crescentus* paracrystalline surface layer protein. *Canadian journal of microbiology* **38**, 193-202 (1992).

20 Linhartova, I. *et al.* RTX proteins: a highly diverse family secreted by a common mechanism. *FEMS microbiology reviews* **34**, 1076-1112, doi:10.1111/j.1574-6976.2010.00231.x (2010).

21 Smit, J., Engelhardt, H., Volker, S., Smith, S. H. & Baumeister, W. The S-layer of *Caulobacter crescentus*: three-dimensional image reconstruction and structure analysis by electron microscopy. *Journal of bacteriology* **174**, 6527-6538 (1992).

22 Fagan, R. P. *et al.* Structural insights into the molecular organization of the S-layer from *Clostridium difficile*. *Molecular microbiology* **71**, 1308-1322, doi:10.1111/j.1365-2958.2009.06603.x (2009).

23 Kern, J. *et al.* Structure of surface layer homology (SLH) domains from *Bacillus anthracis* surface array protein. *The Journal of biological chemistry* **286**, 26042-26049, doi:10.1074/jbc.M111.248070 (2011).

24 Pavkov, T. *et al.* The structure and binding behavior of the bacterial cell surface layer protein SbsC. *Structure* **16**, 1226-1237, doi:10.1016/j.str.2008.05.012 (2008).

25 Rasmussen, S. G. *et al.* Crystal structure of the beta2 adrenergic receptor-Gs protein complex. *Nature* **477**, 549-555, doi:10.1038/nature10361 (2011).

26 Domanska, K. *et al.* Atomic structure of a nanobody-trapped domain-swapped dimer of an amyloidogenic beta2-microglobulin variant. *Proceedings of the National Academy of*

Sciences of the United States of America **108**, 1314-1319, doi:10.1073/pnas.1008560108 (2011).

27 Lam, A. Y., Pardon, E., Korotkov, K. V., Hol, W. G. & Steyaert, J. Nanobody-aided structure determination of the EpsI:EpsJ pseudopilin heterodimer from Vibrio vulnificus. *Journal of structural biology* **166**, 8-15, doi:10.1016/j.jsb.2008.11.008 (2009).

28 Fernandez-Escamilla, A. M., Rousseau, F., Schymkowitz, J. & Serrano, L. Prediction of sequence-dependent and mutational effects on the aggregation of peptides and proteins. *Nature biotechnology* **22**, 1302-1306, doi:10.1038/nbt1012 (2004).

29 Bingle, W. H., Nomellini, J. F. & Smit, J. Cell-surface display of a *Pseudomonas aeruginosa* strain K pilin peptide within the paracrystalline S-layer of *Caulobacter crescentus*. *Molecular microbiology* **26**, 277-288 (1997).

30 Tu, Z. C., Gaudreau, C. & Blaser, M. J. Mechanisms underlying *Campylobacter fetus* pathogenesis in humans: surface-layer protein variation in relapsing infections. *The Journal of infectious diseases* **191**, 2082-2089, doi:10.1086/430349 (2005).

31 Strom, S. L., Brahamsha, B., Fredrickson, K. A., Apple, J. K. & Rodriguez, A. G. A giant cell surface protein in *Synechococcus* WH8102 inhibits feeding by a dinoflagellate predator. *Environmental microbiology*, doi:10.1111/j.1462-2920.2011.02640.x (2011).

32 Koval, S. F. & Hynes, S. H. Effect of paracrystalline protein surface layers on predation by *Bdellovibrio bacteriovorus*. *Journal of bacteriology* **173**, 2244-2249 (1991).

33 Koval, S. F. *et al. Bdellovibrio exovorus* sp. nov., a novel predator of *Caulobacter crescentus*. *International journal of systematic and evolutionary microbiology*, doi:10.1099/ijs.0.039701-0 (2012).

34 Engelhardt, H. Are S-layers exoskeletons? The basic function of protein surface layers revisited. *Journal of structural biology* **160**, 115-124, doi:10.1016/j.jsb.2007.08.003 (2007).

35 Sara, M. & Sleytr, U. B. Molecular sieving through S layers of *Bacillus stearothermophilus* strains. *Journal of bacteriology* **169**, 4092-4098 (1987).

36 Engelhardt, H. & Peters, J. Structural research on surface layers: a focus on stability, surface layer homology domains, and surface layer-cell wall interactions. *Journal of structural biology* **124**, 276-302, doi:10.1006/jsbi.1998.4070 (1998).

37 Peschel, A. & Sahl, H. G. The co-evolution of host cationic antimicrobial peptides and microbial resistance. *Nature reviews. Microbiology* **4**, 529-536, doi:10.1038/nrmicro1441 (2006).

38 Jenssen, H., Hamill, P. & Hancock, R. E. Peptide antimicrobial agents. *Clinical microbiology reviews* **19**, 491-511, doi:10.1128/CMR.00056-05 (2006).

39 Gilchrist, A. & Smit, J. Transformation of freshwater and marine *caulobacters* by electroporation. *Journal of bacteriology* **173**, 921-925 (1991).

40 Evinger, M. & Agabian, N. Envelope-associated nucleoid from *Caulobacter crescentus* stalked and swarmer cells. *Journal of bacteriology* **132**, 294-301 (1977).

41 Poindexter, J. S. Biological Properties and Classification of the *Caulobacter* Group. *Bacteriological reviews* **28**, 231-295 (1964).

42 Toporowski, M. C., Nomellini, J. F., Awram, P., Levi, A. & Smit, J. Transcriptional regulation of the S-layer protein type I secretion system in *Caulobacter crescentus*. *FEMS microbiology letters* **251**, 29-36, doi:10.1016/j.femsle.2005.07.028 (2005).

43 Sambrook, J., Fritsch, E. F. & Maniatis, T. *Molecular cloning : a laboratory manual*. 2nd edn, (Cold Spring Harbor Laboratory, 1989).

44 Walker, S. G., Smith, S. H. & Smit, J. Isolation and comparison of the paracrystalline surface layer proteins of freshwater *caulobacters*. *Journal of bacteriology* **174**, 1783-1792 (1992).

45 Ghassabeh Hassanzadeh, G., Saerens, D. & Muyldermans, S. in *Antibody Engineering. Vol. 2* (eds Roland Kontermann, Stefan Dübel, & Springer Protocols) 1 online resource (Springer, 2010).

46 Wiegand, I., Hilpert, K. & Hancock, R. E. Agar and broth dilution methods to determine the minimal inhibitory concentration (MIC) of antimicrobial substances. *Nature protocols* **3**, 163-175, doi:10.1038/nprot.2007.521 (2008).

47 de la Fuente-Nunez, C. *et al.* Inhibition of bacterial biofilm formation and swarming motility by a small synthetic cationic peptide. *Antimicrobial agents and chemotherapy*, doi:10.1128/AAC.00064-12 (2012).

48 Chayen, N. E. & Saridakis, E. Protein crystallization: from purified protein to diffraction-quality crystal. *Nature methods* **5**, 147-153, doi:10.1038/nmeth.f.203 (2008).

49 Mueller, M., de la Pena, A. & Derendorf, H. Issues in pharmacokinetics and pharmacodynamics of anti-infective agents: kill curves versus MIC. *Antimicrobial agents and chemotherapy* **48**, 369-377 (2004).

50 Campos, M. A. *et al.* Capsule polysaccharide mediates bacterial resistance to antimicrobial peptides. *Infection and immunity* **72**, 7107-7114, doi:10.1128/IAI.72.12.7107-7114.2004 (2004).

51 Szafranski-Schneider, E. *et al.* Msb2 Shedding Protects *Candida albicans* against Antimicrobial Peptides. *PLoS pathogens* **8**, e1002501, doi:10.1371/journal.ppat.1002501 (2012).

52 Yang, L. Y., Pei, Z. H., Fujimoto, S. & Blaser, M. J. Reattachment of surface array proteins to *Campylobacter fetus* cells. *Journal of bacteriology* **174**, 1258-1267 (1992).

53 Pavkov-Keller, T., Howorka, S. & Keller, W. The structure of bacterial S-layer proteins. *Progress in molecular biology and translational science* **103**, 73-130, doi:10.1016/B978-0-12-415906-8.00004-2 (2011).